LA-UR-21-24059
Approved for public release; distribution is unlimited.

Title: Simulations of SITI Cookoff Experiments Carried Out with Different Lots of PBX 9502

Author(s): Aviles-Ramos, Cuauhtemoc

Intended for: Report

Issued: 2021-04-27

Simulations of SITI Cookoff Experiments Carried Out with Different Lots of PBX 9502

Aviles-Ramos, C.

Los Alamos National Laboratory, W-13
Los Alamos, New Mexico 87545

Abstract

A pressure dependent cookoff model for PBX 9502 was developed by Hobbs' et. al. [1]. PBX 9502 is composed of 95% by mass triaminotrinitrobenzene (TATB) and a 5% by mass chlorotrifluoroethylene/vinylidine fluoride binder. The objective in this study is to implement this cookoff model in Aria [2] to simulate Sandia Instrumented Thermal Ignition (SITI) experiments that were carried out with different manufacturing lots of PBX 9502. The SITI design consists of solid cylinders (1" diameter × 1" height) of insensitive high explosive (IHE) confined by a cylindrical aluminum case. An electric heater is wrapped around the lateral surface of the case. This heater produces a temperature heating ramp on the outer surface of the case. Internal thermocouples measure the IHE temperature rise from the center to locations close to the IHE-aluminum interface. The energetic material is heated until thermal ignition occurs. Pressure is measured with a static pressure transducer installed on top of the confinement case. Two–dimensional axisymmetric heat conduction finite element models were implemented to simulate these experiments using four options of the PBX 9502 cookoff model [1]. In addition, the predictive ability of this thermal decomposition model is evaluated using Latin Hypercube Sampling (LHS) techniques.

SITI Experiments Description and Observations

Table 1 summarizes the sealed SITI experiments carried out so far. Figure 1 shows the design of the SITI apparatus [3]. Figure 2 depicts the internal thermocouple locations on the mid-plane. Figure 3 shows internal temperature measurements at the center thermocouple and the boundary condition thermocouples for SITI experiment # 877. Measurements like the ones shown in Fig. 4 are used as boundary conditions to carry out simulations and comparisons with the finite element model response in the mid-plane of the IHE. The mid-plane is located between the two IHE solid cylinders shown in Fig. 1. Each aluminum cell contains one solid cylinder (1" diameter × ½" height). These cylinders come together at the mid-plane and the thermocouple wires are installed

Table 1. SITI experiments carried out with three lots of PBX 9502

SITI #	Manufacturing Lot #	Ullage, %	Set Point, °C	Second Ramp?	Experimental Time to Ignition, s
873	HOL89E891-010	25	260	No	14034
874	HOL89E891-010	25	290	Yes	4730
875	HOL89E891-010	25	280	No	6696
876	HOL89E891-010	25	265	No	11752
877	HOL89E891-010	18.7	260	Yes	10881
878	HOL88A891-006	18.7	264	Yes	8450
880	HOL88B891-007	18.7	260	Yes	22417

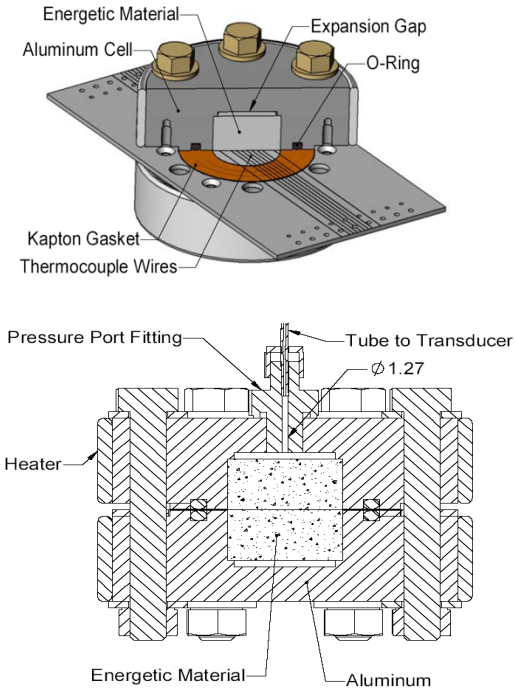

Figure 1. Sandia Instrumented Thermal Ignition apparatus [3].

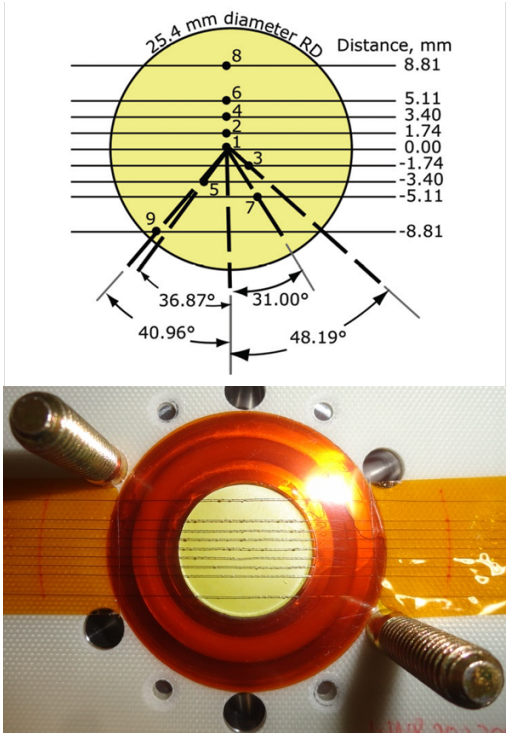

Figure 2. Internal mid-plane thermocouples for SITI apparatus [3].

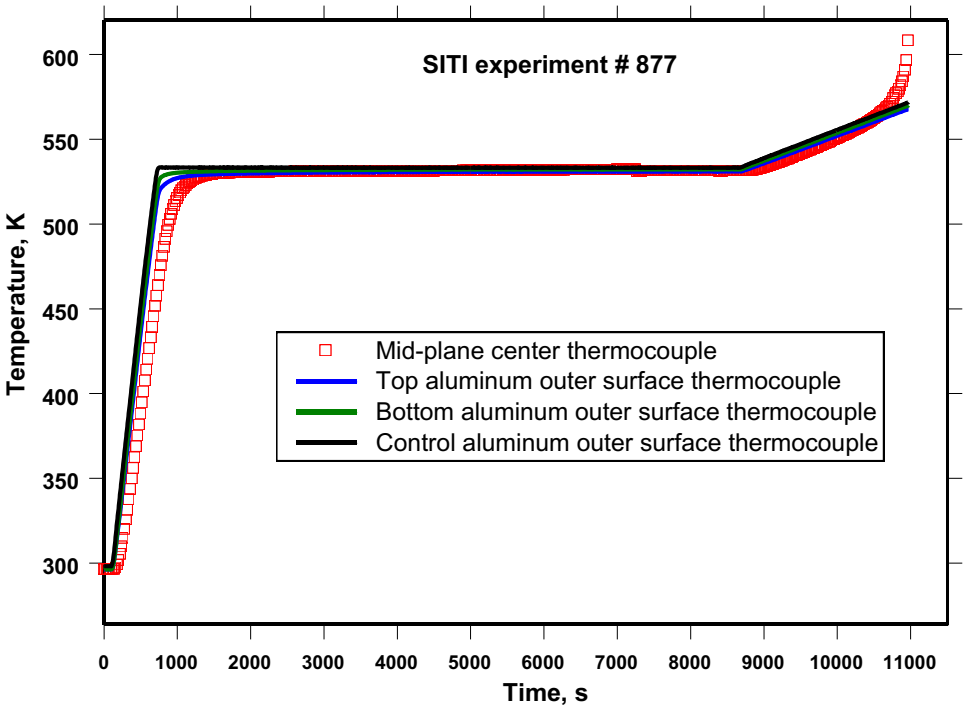

Figure 3. Temperature readings of boundary conditions thermocouples and the PBX 9502 center thermocouple.

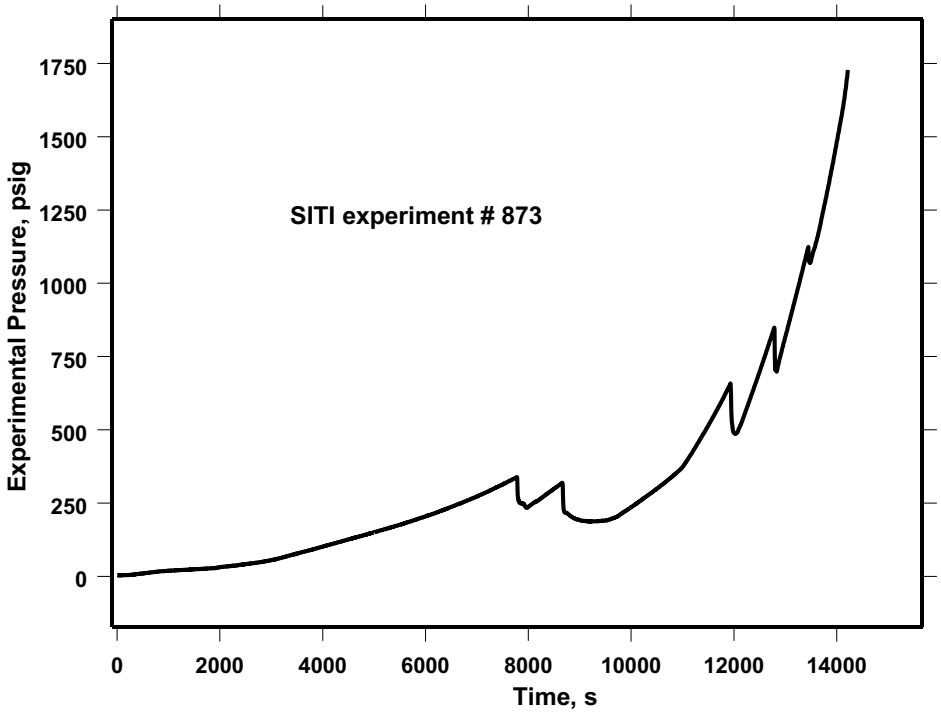

Figure 4. Static pressure measured in STI experiment #873.

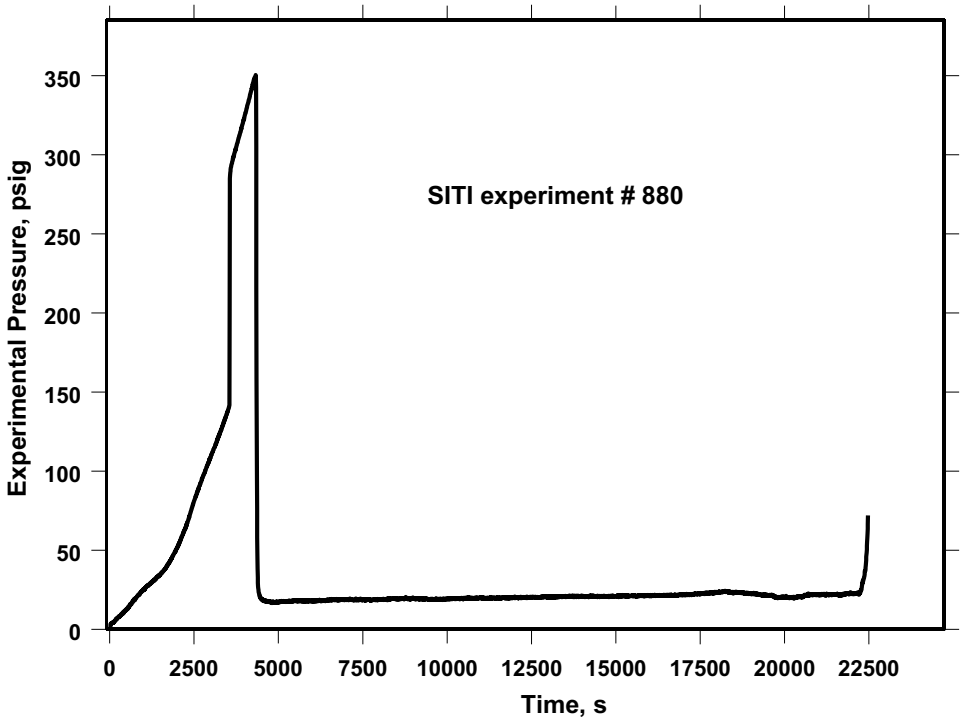

Figure 5. Static pressure measured in STI experiment #880

between them. Note from Fig. 3 that the aluminum case is heated up to a setpoint temperature (ST) of 533 K. Once the outer surface of the aluminum case reaches 533 K, it is kept at a constant temperature close to 533 K by controlling the power to the electric heaters. When time reaches 8670 s, an additional heating ramp is applied by increasing the power to the electric heater. Also, note from Fig. 3 that the temperature measured by the center thermocouple begins to increase between 10190 s and 10700 s. This is an indication that the PBX 9502 thermal decomposition reactions begin to generate more energy and are already producing a significant amount of energy. For times greater or equal than 10700 seconds, temperatures at the center of the PBX 9502 sample are already greater than the aluminum case boundary temperatures indicating an even higher amount of energy generated by the thermal decomposition reactions. Eventually, the central temperature begins to increase very rapidly leading to a thermal explosion.

The PBX 9502 is interesting in that the gases are retained within the explosive, until the material fractures. Figure 4 shows the pressure measured in SITI #873. This figure shows that the experiment leaked at ~7680 s, after this time the pressure continued to increase with slight decreases but it had a global increase up to 1728 psi at ignition. The measured pressure in SITI experiment #880 is shown in Fig. 5. It seems from this pressure curve that SITI #880 developed a leak at around ~4400 s. These anomalies make the modeling of these experiments more challenging. This is why it was decided to use the four options of the PBX 9502 cookoff model described in reference [1] to simulate these experiments.

Description of the PBX 9502 Cookoff Model

The conductive energy equation in the PBX 9502 cylinders was used to model the decomposition process associated with the cook-off of the IHE. A PBX 9502 pressure dependent thermal decomposition model developed by Hobbs' et al. [3] was used to define a volumetric

source term in the PBX 9502 heat conduction equation. This model considers 4 reaction steps in a global mechanism that defines the decomposition of PBX 9502. The first reaction considers drying of the PBX, where the mass fraction of adsorbed water is small. The second reaction involves elimination of a water molecule from TATB to form mono-furazan (MF), which subsequently decomposes into stable reaction products. The final reaction is direct decomposition of TATB to form equilibrium products. The four-step mechanism reads [1]:

1. $H_2O_a \rightarrow H_2O_g$
2. $TATB \rightarrow MF + H_2O_m$
3. $MF \rightarrow 6.52\ Gas_m + 4.18\ Carbon_m$
4. $TATB \rightarrow 7.5\ Gas_t + 3.9\ Carbon_t$

where subscript *a* means adsorbed, subscript *g* means gaseous, subscript *m* means coming from the mono-furazan decomposition, and subscript *t* means coming from the TATB decomposition. The reaction rates associated with the four reaction steps assume first order reactions [1]

$$r_1 = A_1 \exp\left(\frac{-E_1 \pm \xi_1 \sigma_1}{RT}\right)\left[H_2O_a\right] \tag{7}$$

$$r_2 = A_2 \exp\left(\frac{-E_2}{RT}\right)\left[TATB\right] \tag{8}$$

$$r_3 = A_3 \exp\left(\frac{-E_3}{RT}\right)\left[MF\right] \tag{9}$$

$$r_4 = A_4\left(\frac{P}{P_0}\right)^e T^{-3} \exp\left(\frac{-E_4 \pm \xi_4 \sigma_4}{RT}\right)\left[TATB\right] \tag{10}$$

where the species concentrations in square brackets [.] are in kgmol/m^3, $e = 0.7$, E_i (i = 1, … ,4) are the activation energies, A_i (i = 1,…,4) are the pre-exponential factors, ξ_i =*normsinv*(P_i) (i = 1 and 4) is a distribution parameter represented by the inverse of the normal distribution of the progress of reaction steps 1 and 4

$$P_1 = \frac{M_{wH_2O_a}\left[H_2O_a\right]}{\omega_{H_2O_a}\ \rho_{b,0}} \qquad P_4 = \frac{M_{wTATB}\left[TATB\right]}{(1-\omega_{H_2O_a})\ \rho_{b,0}} \tag{11}$$

where $\omega_{H_2O_a}$ is the mass fraction of adsorbed water, $\rho_{b,0}$ is the initial bulk density of PBX 9502, $M_{wH_2O_a}$ and M_{wTATB} are the molecular weights of water and TATB. The parameters σ_i (i = 1 and 4) are the standard deviations of the activation energies E_i (i = 1 and 4), R is the universal gas constant, and $(P/P_0)^{0.7}$ is pressure dependent ratio introduced to make the direct decomposition of TATB pressure dependent. The parameter P_0 is the initial pressure, and P is the average pressure in the PBX 9502 calculated using the equation

$$P = \frac{z\, n\, R\, T_{ave}}{V_g} \tag{12}$$

where z is the compressibility factor calculated using the BKW equation of state [4] defined by Eq. (13), n is the total number of moles of gases produced by the reactions defined by Eq. (14), T_{ave} is an integral average of the temperature in the PBX 9502 defined by Eq. (15), and V_g which is defined by Eq. (16) is the volume occupied by the decomposition gases

$$z = 1 + \frac{n\kappa \sum n_i k_i}{V_g\,(T_{ave} + \Theta)^{\alpha}} \exp\left(\beta \frac{n\kappa \sum n_i k_i}{V_g\,(T_{ave} + \Theta)^{\alpha}} \right) \tag{13}$$

where κ, n_i, k_i, Θ, and α are BKW parameters defined in reference [5].

$$n = \int_V \left([H_2O_g] + [H_2O_m] + [Gas_m] + [Gas_t] \right) dV \tag{14}$$

$$T_{ave} = \frac{\int_V T\, dV}{\int_V dV} \tag{15}$$

$$V_g = \int_V \varphi\, dV \tag{16}$$

where ϕ is the gas volume fraction defined by

$$\phi = 1 - \frac{S_f\, \rho_{c,0} (1 - \phi_0)}{\rho_c} \tag{17}$$

where ρ_c, $\rho_{c,0}$, ϕ_0, and S_f are the condensed density, Eq. (19), initial condensed density, initial gas volume fraction, and reacted solid fraction (Eq. (18)) respectively

$$S_f = \frac{M_{wH_2O_a}[H_2O_a] + M_{wTATB}[TATB] + M_{wMF}[MF] + M_{wC}[Carbon_m] + M_{wC}[Carbon_t]}{\rho_{b,0}} \tag{18}$$

where M_{wMF} and M_{wC} are the molecular weights of mono-furazan and carbon respectively. The condensed density is defined as

$$\rho_c = \rho_{c,0} \left[1 - \beta_V (T - T_0) \right] \tag{19}$$

where T_0 is the initial temperature and β_V is the thermal expansion coefficient [5] defined by Eq. (20). The decrease in ρ_c is limited by the value of the bulk density ρ_b.

$$\beta_V = 99 \times 10^{-6} + 0.74 \times 10^{-6}\, T \tag{20}$$

The values of the parameters appearing in Eqs. (7)–(20) are given in reference [1]. The system of partial differential equations (PDEs) that involve the chemistry and conductive energy equations solved by Aria [2] in the PBX 9502

$$\frac{\partial [H_2O_a]}{\partial t} = -r_1 \tag{21}$$

$$\frac{\partial[H_2O_g]}{\partial t} = r_1 \tag{22}$$

$$\frac{\partial[TATB]}{\partial t} = -r_2 - r_4 \tag{23}$$

$$\frac{\partial[MF]}{\partial t} = r_2 - r_3 \tag{24}$$

$$\frac{\partial[H_2O_m]}{\partial t} = r_2 \tag{25}$$

$$\frac{\partial[Gas_m]}{\partial t} = 6.52\, r_3 \tag{26}$$

$$\frac{\partial[Carbon_m]}{\partial t} = 4.18\, r_3 \tag{27}$$

$$\frac{\partial[Gas_t]}{\partial t} = 7.5\, r_4 \tag{28}$$

$$\frac{\partial[Carbon_t]}{\partial t} = 3.90\, r_4 \tag{29}$$

$$\rho_b\, C_b \frac{\partial T}{\partial t} = \nabla \bullet (k\, \nabla T) + \sum_{i=1}^{4} r_i\, h_{r_i} M_{w,i} \tag{30}$$

where ρ_b and C_b are the bulk density and heat capacity [6] respectively, k is the thermal conductivity as a function of temperature [7], h_{r_i} (i = 1,…,4) is the reaction enthalpy for reaction steps 1–4 [3], and $M_{w,i}$ (i = 1,…,4) are the molecular weights for H_2O_a, *TATB*, *MF*, and *TATB* respectively. The FE code Aria uses an operator splitting technique [8] to solve the system of PDEs represented by Eqs. (21)–(30). This technique considers that Eqs. (21)–(29) are defined locally as ordinary differential equations (ODEs) at the finite elements integration points. The species concentrations are viewed as state variables and this system of ODEs is integrated on an element-by-element basis at each FE time step, Δt_{FE}. A chemistry time step, $\Delta t_{chem.}$, is selected to integrate the system of ODEs represented by the mass conservation equations, (21)–(29), at the finite elements integration (Gauss) points. Aria contains ODE solvers applied to integrate Eqs. (21)–(29).

Four Model Options for Volume Changes in PBX 9502 During Cookoff

Model option 1 is used when there is no damage in the PBX and the bulk volume remains unchanged. This model option is implemented defining the volume of the decomposition gases equal to the volume integral of the gas volume fraction defined by Eq. (16) which is calculated from the decomposition chemistry. The volume changes due to swelling caused by temperature increases and gas generation is set equal to zero for this option and the thermal decomposition gases are assumed to stay in the PBX which experiences closed pore decomposition.

Model option 2 is defined when there is no damage in the PBX and it experiences swelling due to thermal expansion effects. A swelling model that considers thermal expansion given in reference [4] has the form

$$\Delta \mathrm{V}_2 \approx \frac{0.11\ \mathrm{V}_{\mathrm{EM}}\ \left(T_{ave} - T_0\right)}{\left(530 - T_0\right)} \tag{31}$$

where V_{EM} is the volume of the energetic material. The PBX 9502 kinetic model assumes that reactions start at around 530 K. Equation (31) accounts for the bulk volume change of the PBX 9502 due to thermal expansion effects only. The increase in volume defined by Eq. (31) increases the bulk volume of the pores that are present in the PBX 9502. The volume change defined by Eq. (31) affects the calculation of the pressure through the augmentation of the volume occupied by the gases inside the PBX pores. So, model option 2 involves the calculation of the pressure using

$$P = \frac{z\ n\ R\ T_{ave}}{\int_V \varphi\, dV + \dfrac{0.11\ \mathrm{V}_{\mathrm{EM}}\ \left(T_{ave} - T_0\right)}{\left(530 - T_0\right)}} \tag{32}$$

Eq. (32). Note that reaction rate r_4 which involves the direct decomposition of TATB in Eq. (10) will decrease due to inclusion of Eq. (31) in the denominator of Eq. (12). This inclusion will cause a pressure decrease and consequently a decrease in the reaction rate r_4.

Model option 3 is defined when there is no damage in the PBX and it experiences swelling due to thermal expansion and gas generation effects. Reference [4] defined a swelling model due to thermal expansion and gas generation given by the following equation. So, for the model option 3

$$\Delta \mathrm{V}_3 \approx \begin{cases} \dfrac{0.11\ \mathrm{V}_{\mathrm{EM}}\ \left(T_{ave} - T_0\right)}{\left(530 - T_0\right)} & \text{for } T \le 530 \text{ K} \\ \\ \mathrm{V}_{\mathrm{EM}}\ \left(0.008\ T_{ave} - T_0\right) & \text{for } T > 530 \text{ K} \end{cases} \tag{33}$$

the pressure is calculated using Eq. (34)

$$P = \frac{z\ n\ R\ T_{ave}}{\int_V \varphi\, dV + \Delta \mathrm{V}_3} \tag{34}$$

where $\Delta \mathrm{V}_3$ is defined by Eq. (33). At the onset of the thermal decomposition reactions that happens around 530 K, the swelling model defined by Eq. (33) continues to increase the volumes of the pores. This volume increase is due to the generation of thermal decomposition gases. It is asummed that the PBX 9502 doesn't experience damage for model options 1, 2, and 3. If the PBX 9502 is under confinement and it experiences damage through fracture or crack formation, an additional model option was defined in reference [3]. This is model option 4 which considers that the PBX 9502 is under confinement and that this confinement contains an internal void space or ullage where the thermal decomposition gases ecaping the damaged PBX can flow and expand. This ullage is filled by the decomposition gases and needs to be added to the total volume used in model option 2. So, the pressurization equation for model option 4 can be defined by Eq. (35) where $\mathrm{V}_{\mathrm{Ullage}}$ is the internal void volume inside the confinement. It is pointed out that the compressiblity

$$P = \frac{z\ n\ R\ T_{ave}}{\int_V \varphi\, dV + \dfrac{0.11\ \mathrm{V_{EM}}\ \left(T_{ave} - T_0\right)}{\left(530 - T_0\right)} + \mathrm{V_{Ullage}}} \tag{35}$$

factor defined by Eq. (13) also needs to be modified to calculate the pressure for model options 2, 3, and 4 because it contains the term V_g. So, for model options 2, 3, and 4 the compressibility factor takes the form of Eqs. (36), (37), and (38) respectively. The four model options defined here

$$z = 1 + \frac{n\kappa \sum n_i k_i}{\left(V_g + \Delta \mathrm{V_2}\right)(T_{ave} + \Theta)^{\alpha}} \exp\left(\beta \frac{n\kappa \sum n_i k_i}{\left(V_g + \Delta \mathrm{V_2}\right)(T_{ave} + \Theta)^{\alpha}} \right) \tag{36}$$

$$z = 1 + \frac{n\kappa \sum n_i k_i}{\left(V_g + \Delta \mathrm{V_3}\right)(T_{ave} + \Theta)^{\alpha}} \exp\left(\beta \frac{n\kappa \sum n_i k_i}{\left(V_g + \Delta \mathrm{V_3}\right)(T_{ave} + \Theta)^{\alpha}} \right) \tag{37}$$

$$z = 1 + \frac{n\kappa \sum n_i k_i}{\left(V_g + \Delta \mathrm{V_2} + \mathrm{V_{Ullage}}\right)(T_{ave} + \Theta)^{\alpha}} \exp\left(\beta \frac{n\kappa \sum n_i k_i}{\left(V_g + \Delta \mathrm{V_2} + \mathrm{V_{Ullage}}\right)(T_{ave} + \Theta)^{\alpha}} \right) \tag{38}$$

are useful to gain insight into the simulations of the PBX 9502 SITI experiments. One can compare the predicted thermal ignition times calculated using the four model options with the experimental ignition time obtained in the SITI experiments. The model option that produces the best prediction of the thermal ignition time would be the most likely scenario for the experiment.

Simulation of SITI Experiments Using the Four Cookoff Model Options for PBX 9502

The SITI experiments listed in Table 1 were simulated using the four model options discussed in the previous section. Axisymmetric FE models of the SITI experiments shown in Table 1 were constructed in the heat transfer code Aria [2]. Input files were written to implement the four model options and the boundary conditions for the seven experiments shown in Table 1. Figures 6 and 7 show the axisymmetric SITI meshes for ullages of 25% and 18.7% respectively. Table 2 shows the results of these simulations.

Table 2 shows that model option 3 produced the best prediction of the thermal ignition time for SITI 873 with an error of 1.4%. This means that the PBX 9502 didn't experience damage and it swelled due to thermal expansion and gas generation effects. The best prediction of the thermal ignition time percentage error, -19.5%, for SITI 874 in Table 2 was obtained when option 4 of the model was used. This is an indication that the PBX 9502 in SITI 874 experienced damage due to fracture or crack formation. This caused the decomposition gases to escape the PBX 9502 and flow into the expansion gaps. The simulation results in Table 2 for SITI 875 show that the smallest thermal ignition time percentage error was -9.1%. This was achieved with model option 4. So, for this case the PBX 9502 also experienced damage and the expansion gaps were filled with thermal decomposition gases. The simulation of SITI test 876 that produced the best prediction was the one that predicted thermal ignition time with a percentage error of -7.2% when model option 3 was

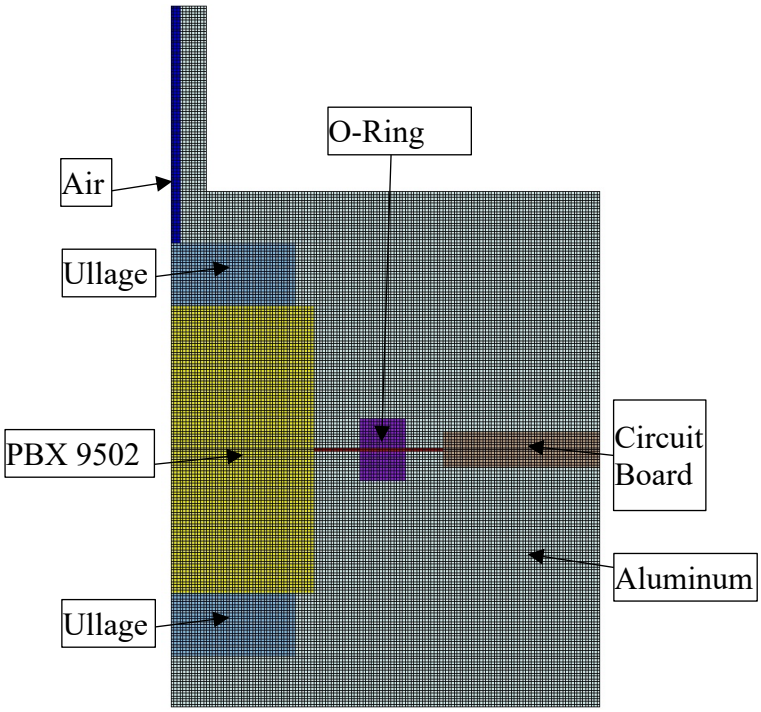

Figure 7. Mesh of SITI with 25 % ullage.

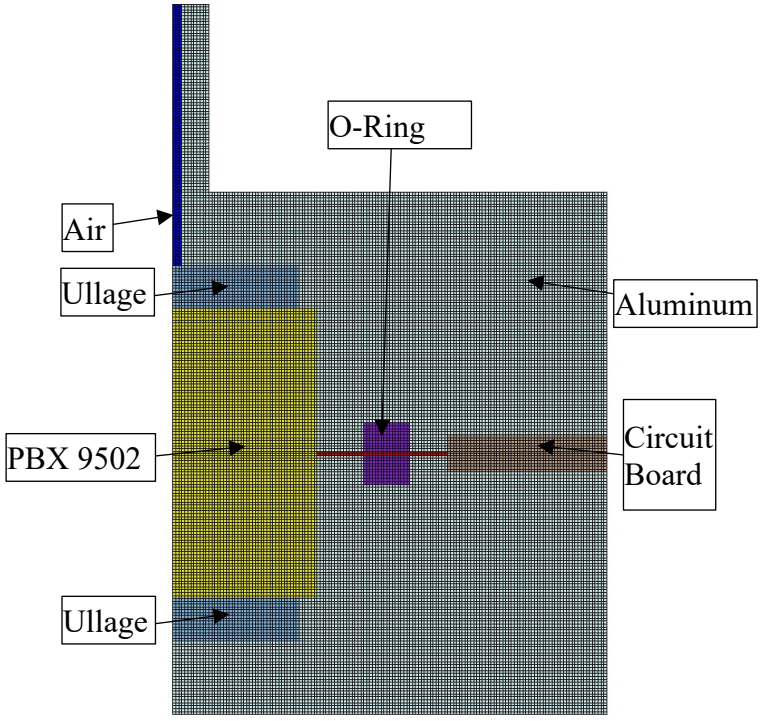

Figure 7. Mesh of SITI with 18.7 % ullage.

Table 2. Experimental and predicted thermal ignition times using Hobbs' PBX 9502 model. The SITI tests in Table 1 are simulated using the four model options defined in reference [1].

SITI #	Ullage, %	Set Point, ºC	Model Option	Experimental Time to Ignition, s	Predicted Time to Ignition, s	Error, %
873	25	260	1	14034	1731	-87.7
873	25	260	2	14034	13247	-5.6
873	**25**	**260**	**3**	**14034**	**14235**	**1.4**
873	25	260	4	14034	20656	47.2
874	25	290	1	4730	878	-81.4
874	25	290	2	4730	2875	-39.2
874	25	290	3	4730	3768	-20.3
874	**25**	**290**	**4**	**4730**	**3809**	**-19.5**
875	25	280	1	6696	1025	-84.7
875	25	280	2	6696	4398	-34.3
875	25	280	3	6696	5747	-14.2
875	**25**	**280**	**4**	**6696**	**6088**	**-9.1**
876	25	265	1	11748	1353	-88.5
876	25	265	2	11748	9197	-21.7
876	**25**	**265**	**3**	**11748**	**10896**	**-7.2**
876	25	265	4	11748	13940	18.7
877	18.7	260	1	10881	1672	-84.6
877	18.7	260	2	10881	10449	-3.97
877	18.7	260	3	10881	11095	1.96
877	**18.7**	**260**	**4**	**10881**	**11040**	**1.46**
878	18.7	264	1	8450	1710	-79.8
878	**18.7**	**264**	**2**	**8450**	**8623**	**2.0**
878	18.7	264	3	8450	9304	10.1
878	18.7	264	4	8450	9130	8.0
880	18.7	260	1	22417	1657	-92.6
880	18.7	260	2	22417	12926	-42.3
880	18.7	260	3	22417	14044	-37.3
880	18.7	260	4	22417	18069	-19.4
880	**18.7**	**260**	**Experimental Pressure[a]**	**22417**	**24399**	**8.8**

[a] Pressure P in Eq. (10) 5 is substituted by the experimental pressure shown in Fig. 5. This pressure data is used instead of calculating pressure using the equation of state given by Eq. (12).

used. This means that the PBX 9052 didn't experience damage but it did experience swelling due to thermal expansion and gas generation due to decomposition. The simulation of SITI 877 that produced the smallest percentage error of 1.46% was the one carried out with model option 4. This means that for this case the PBX 9502 experienced fracture or crack formation and the thermal decomposition gases flowed into the expansion gaps. The simulation of SITI 878 that used model option 2 produced the smallest percentage error of 2.0%. This means that for this case the PBX 9502 didn't experience damage but it did experience swelling due to thermal expansion effects. The measured pressure for SITI 880 in Fig. 5 shows that this experiment leaked. Figure 5 shows that the pressure increased up to around 350 psig and then it dropped probably due to a leak. For the case of SITI 880, the measured pressure was substituted into Eq. (10) to carry out the simulation that produced the smallest ignition time percentage error of 8.8%. Note that when the experimental pressure is used, the cookoff model becomes independent of the model options. The model options affect the calculation of pressure and when the measured pressure is substituted in Eq. (10), the reaction rate r_4 is not affected by the choice of a model option because the pressure calculated by this option is not used in Eq. (10). Table 3 shows the model options that produced the best predictions. Also, it shows the measured and calculated time-to-ignition as well as the percentage

Table 3. Experimental and predicted thermal ignition times using Hobbs' PBX 9502 model. Each simulation listed used the model option that produced the best prediction of the thermal ignition time percentage error in Table 2.

SITI #	Ullage, %	Set Point, °C	Model Option	Experimental Time to Ignition, s	Predicted Time to Ignition, s	Error, %
873	25	260	3	14034	14235	1.4
874	25	290	4	4730	3809	-19.5
875	25	280	4	6696	6088	-9.1
876	25	265	3	11748	10896	-7.2
877	18.7	260	4	10881	11040	1.5
878	18.7	264	2	8450	8623	2.0
880	18.7	260	Experimental Pressure[a]	22417	24399	8.8

[a] Pressure P in Eq. (10) is substituted by the experimental pressure shown in Fig. 5. This pressure data is used instead of calculating pressure using the equation of state given by Eq. (12).

error. The range of errors is from -19.5% to +8.8% with an average error of -3.1%. The Root Mean Squared Deviation (RMSD) is 923 s and the percent normalized RMSD is 5%. Equations (39) to (31) show how the Error % in Table 3, the RMSD, and the normalized RMSD were calculated where t_c, t_m, and n are the calculated and measured ignition times, and the number of experiments respectively. Figure 8 plots the measured ignition time plotted against the calculated ignition time with a linear correlation coefficient of 0.995. These results show that Hobbs' PBX 9502 cookoff

$$\text{Error} = 100 \times \frac{\left(t_c - t_m\right)}{t_m} \tag{39}$$

$$\text{RMSD} = \sqrt{\frac{\sum_{i=1}^{n}\left(t_{c,i} - t_{m,i}\right)}{n}} \tag{40}$$

$$\text{Normalized RMSD} = 100 \times \frac{\text{RMSD}}{t_m^{\max} - t_m^{\min}} \tag{41}$$

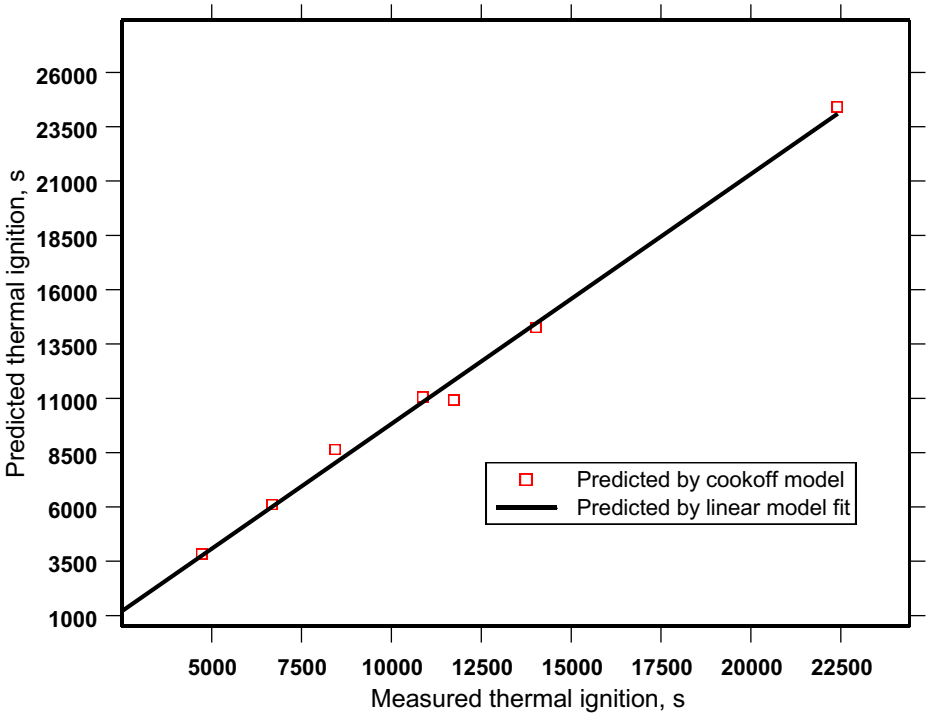

Figure 15. Measured against predicted thermal ignition times for Hobbs' et al. PBX 9502 cookoff model [1]. The correlation coefficient is 0.995.

model continues to be adequate for the manufacturing lots shown in Table 1. The average time-to-ignition prediction percentage error is only -3.1% and the correlation coefficient is close to 1.

Latin Hypercube Sampling Study

An LHS study was carried out for the simulations shown in Table 3. The model options shown in Table 3 were used to carry out this LHS sampling. McKay et al. [9] developed the LHS which is a smart sampling technique similar to a Monte Carlo uncertainty analysis and it is used to propagate uncertainty into the predicted results. The LHS samples used by the model were generated using a sensitivity analysis software called DAKOTA [10] and the values of the parameter uncertainties were taken from reference [1]. The linear standard correlation coefficient (Pearson's correlation coefficient) was used to calculate the correlation strength or sensitivity of the thermal ignition time for each of the uncertain input parameters. Pearson's correlation coefficient is defined by Eq. (42) where μ_t is the

$$r = \frac{\frac{1}{n-1}\sum_{i=1}^{n}\left(t_i - \mu_t\right)\left(y_i - \mu_y\right)}{\sigma_t \times \sigma_y} \tag{42}$$

mean or the average of the computed ignition times for the *n* LHS samples, μ_y is the mean of the LHS inputs for the uncertain variable *y*, σ_t is the standard deviation of the calculated ignition times, and σ_y is the standard deviation of the LHS inputs for the uncertain variable *y*. Table 4 shows the uncertainty multipliers used for this LHS sampling study. Seventeen ignition kinetics parameters were considered for this LHS study. All the uncertainty values were assumed to be uniformly distributed over the given range.

Table 4. Uncertainty multipliers and range for LHS.

Symbols	Description	Value
$U_{\beta V}$	Volumetric expansion	1±0.03
U_{Cb}	Bulk specific heat	1±0.05
U_{h1}	Reaction 1 enthalpy	1±0.01
U_{h2}	Reaction 2 enthalpy*	0±8.6e5
U_{h3}	Reaction 3 enthalpy	1±0.01
U_{h4}	Reaction 4 enthalpy	1±0.01
U_{k}	Thermal conductivity	1±0.05
U_{Po}	Initial Pressure	1±0.01
U_{r1}	Reaction rate 1	1±0.05
U_{r2}	Reaction rate 2	1±0.05
U_{r3}	Reaction rate 3	1±0.05
U_{r4}	Reaction rate 4	1±0.05
$U_{\rho bo}$	Initial bulk density	1±0.02
U_{To}	Initial temperature	1±0.011
$U_{\Sigma niki}$	Avg. BKWS covolume	1±0.01
U_{Vswell}	Swell volume	1±0.10
$U_{\omega h2oa}$	Initial adsorbed water	1±0.75

*This is an uncertainty range

Table 5. Uncertainty multipliers and correlation coefficients for SITI # 873. The most correlated parameters are associated with the uncertainty multipliers $U_{\omega h2oa}$, U_{Vswell}, U_{r2}, and U_{r4}.

Symbols	Description	Value	r^a	r^2
$U_{\beta V}$	Volumetric expansion	1±0.03	-0.130	0.017
U_{Cb}	Bulk specific heat	1±0.05	-0.035	0.001
U_{h1}	Reaction 1 enthalpy	1±0.01	0.021	0.000
U_{h2}	Reaction 2 enthalpy*	0±8.6e5	0.036	0.001
U_{h3}	Reaction 3 enthalpy	1±0.01	0.182	0.033
U_{h4}	Reaction 4 enthalpy	1±0.01	0.026	0.001
U_{k}	Thermal conductivity	1±0.05	-0.029	0.001
U_{Po}	Initial Pressure	1±0.01	0.042	0.002
U_{r1}	Reaction rate 1	1±0.05	0.071	0.005
U_{r2}	Reaction rate 2	1±0.05	**-0.396**	**0.157**
U_{r3}	Reaction rate 3	1±0.05	-0.031	0.001
U_{r4}	Reaction rate 4	1±0.05	**-0.241**	**0.058**
$U_{\rho bo}$	Initial bulk density	1±0.02	-0.033	0.001
U_{To}	Initial temperature	1±0.011	-0.034	0.001
$U_{\Sigma niki}$	Avg. BKWS covolume	1±0.01	0.022	0.000
U_{Vswell}	Swell volume	1±0.10	**0.450**	**0.202**
$U_{\omega h2oa}$	Initial adsorbed water	1±0.75	**-0.754**	**0.568**

*This is an uncertainty range.

[a]This is Pearson's correlation coefficient.

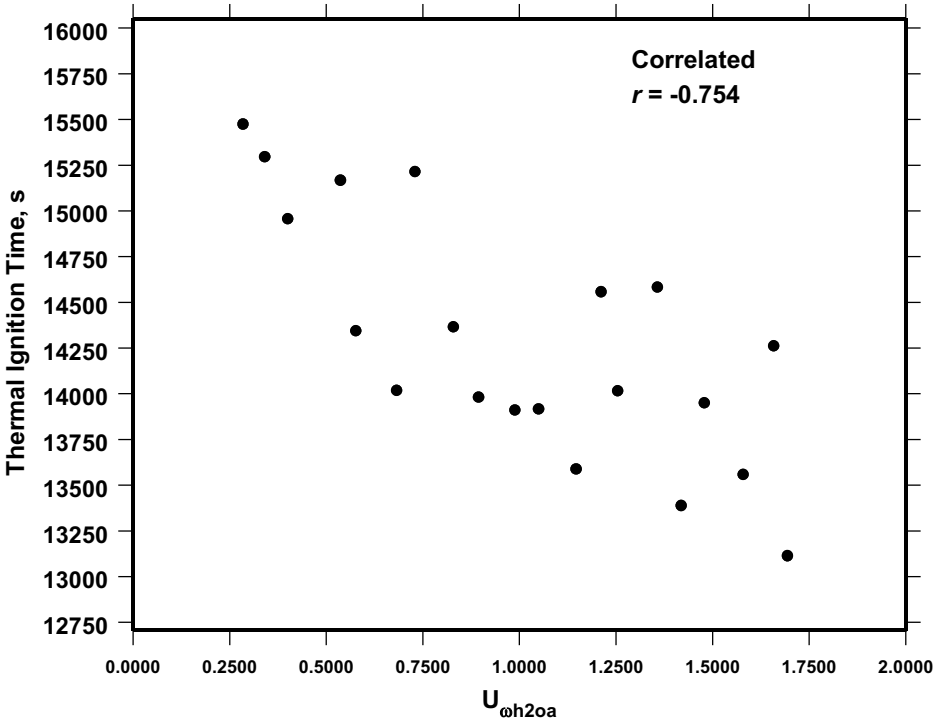

Figure 16. Random variation of the thermal ignition time with the uncertainty multiplier of the initial mass fraction of adsorbed water, $U_{\omega h2oa}$. LHS for SITI experiment 873.

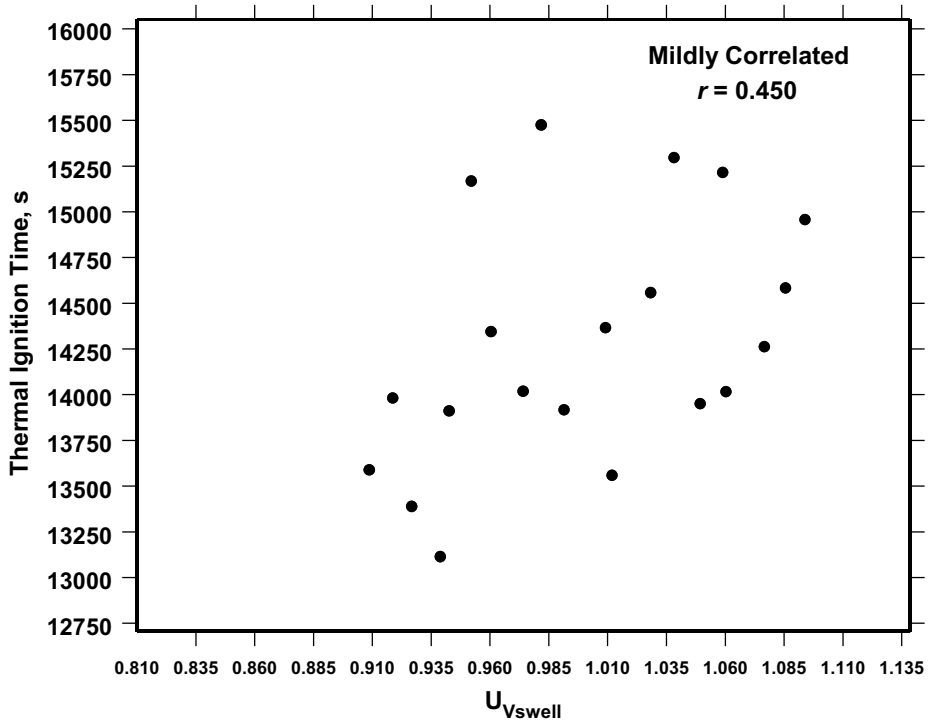

Figure 17. Random variation of the thermal ignition time with the swell volume uncertainty multiplier, U_{Vswell}. LHS for SITI experiment 873.

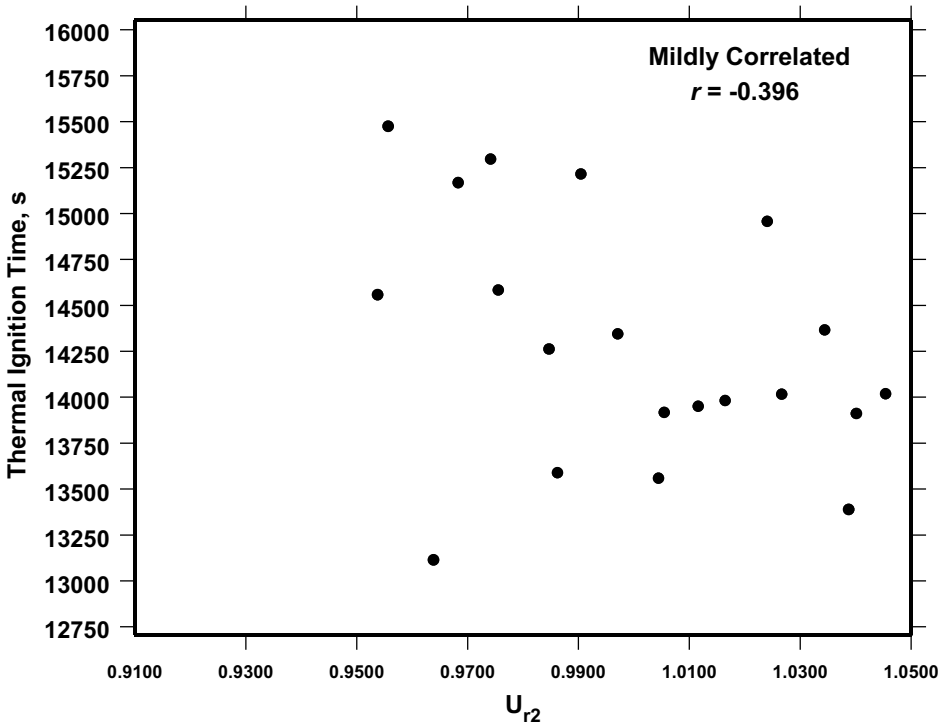

Figure 18. Random variation of the thermal ignition time with the reaction rate 2 uncertainty multiplier, U_{r2}. LHS for SITI experiment 873.

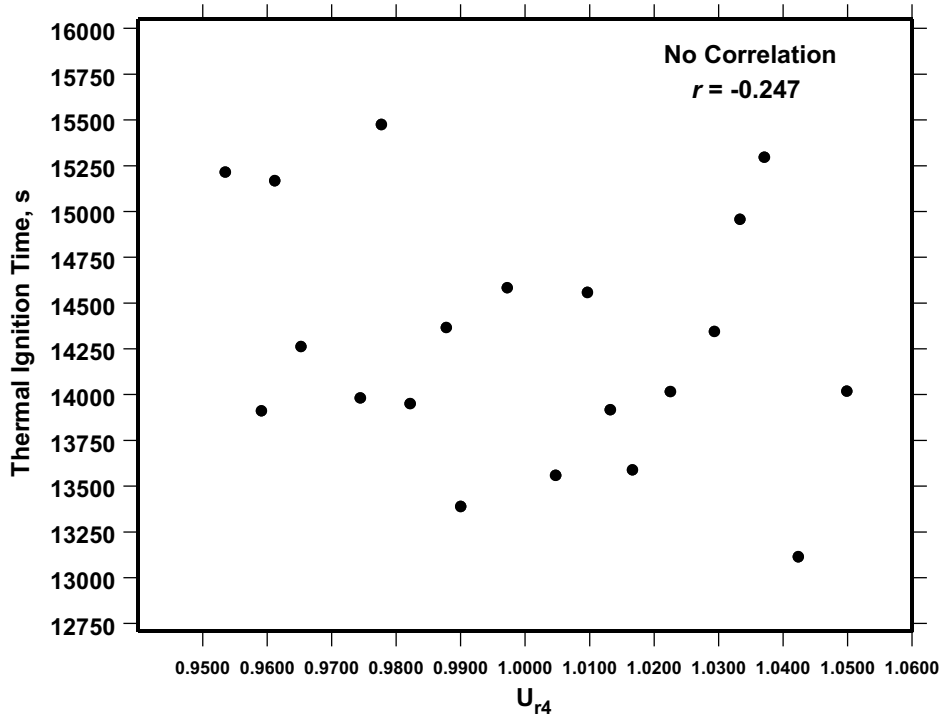

Figure 19. Random variation of the thermal ignition time with the reaction rate 4 uncertainty multiplier, U_{r4}. LHS for SITI experiment 873.

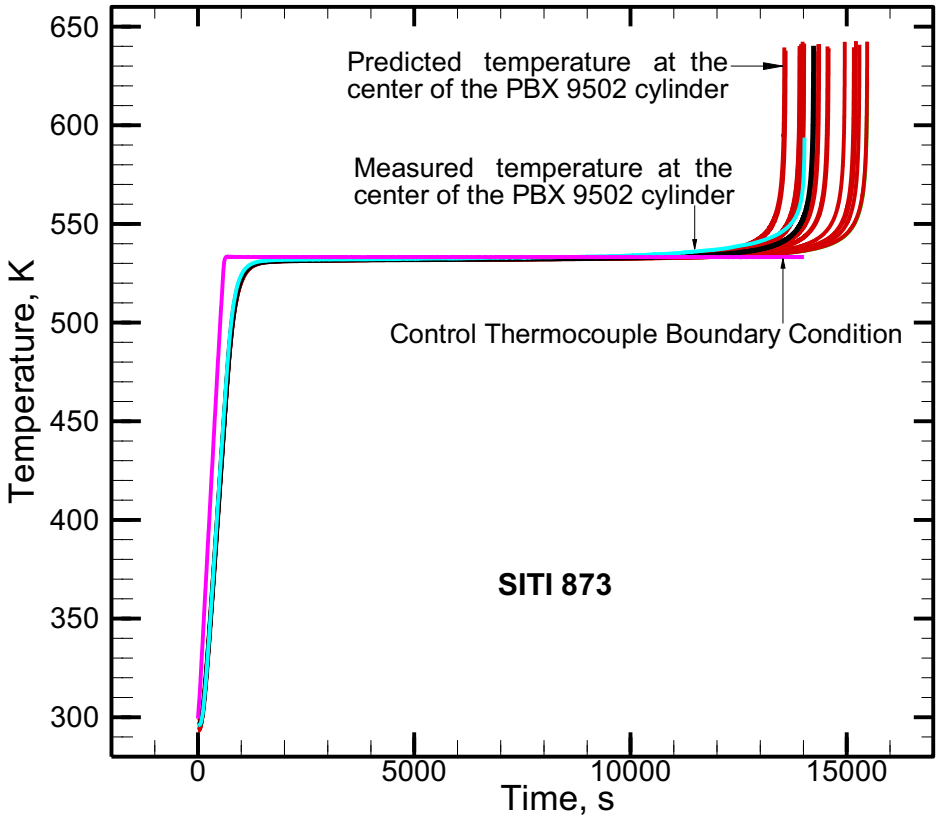

Figure 20. Predicted temperatures for the 20 LHS carried out on SITI experiment 873. The predicted mean center temperature is given in black.

The first LHS sampling study was done on the experiment SITI # 873 using model option 3 as shown in Table 3. Table 5 shows the results that include the Pearson's correlation coefficient for the thermal ignition time. The uncertainty multiplier $U_{\omega h2oa}$ had the highest correlation with a value of -0.754. The sign of this multiplier implies that as the initial adsorbed water mass fraction increases, the time to thermal ignition decreases. Figure 16 plots the time to thermal ignition against $U_{\omega h2oa}$. The swell volume had a correlation coefficient of 0.450 which implies that as the swell volume increases, the thermal ignition time increases. Figure 17 plots the random variation of the thermal ignition time with the swell volume uncertainty multiplier. The reaction rate 2 had a correlation coefficient of -0.396 which implies that as the reaction rate 2 increases, the thermal ignition time decreases. Figure 18 plots the random variation of the thermal ignition time with the reaction rate 2 uncertainty multiplier. The uncertainty multiplier for reaction rate 4, U_{r4}, had a correlation coefficient of -0.241. Figure 19 shows the plot of the thermal ignition time against U_{r4}. Figure 19 shows almost no correlation for the uncertainty multiplier U_{r4}. Figure 20 shows the temperature results for the 20 LHS for the SITI # 873 experiment. This figure also shows the measured and predicted temperatures at the center of the PBX 9502 cylinder, and thermocouple readings of the boundary condition on the lateral surface of the SITI aluminum confinement. The predicted mean of the temperature at the PBX 9502 cylinder is shown in black.

The second LHS sampling study was done on the experiment SITI # 874 using model option 4 as shown in Table 3. Table 6 shows the results that include the Pearson's correlation coefficient for the thermal ignition time. The enthalpy of reaction 2, U_{h2}, had the highest correlation with a value of -0.725. The sign of this range implies that as U_{h2} increases, the thermal ignition time

Table 6. Uncertainty multipliers and correlation coefficients for SITI # 874. The most correlated parameters are associated with the uncertainty multipliers $U_{\omega h2oa}$, U_{r2}, U_{r4}, and the uncertainty range of the enthalpy of reaction 2, U_{h2}.

Symbols	Description	Value	r^a	r^2
$U_{\beta V}$	Volumetric expansion	1±0.03	-0.137	0.019
U_{Cb}	Bulk specific heat	1±0.05	0.074	0.005
U_{h1}	Reaction 1 enthalpy	1±0.01	-0.009	0.000
U_{h2}	Reaction 2 enthalpy*	0±8.6e5	**-0.725**	**0.526**
U_{h3}	Reaction 3 enthalpy	1±0.01	0.117	0.014
U_{h4}	Reaction 4 enthalpy	1±0.01	-0.055	0.003
U_{k}	Thermal conductivity	1±0.05	0.017	0.000
U_{Po}	Initial Pressure	1±0.01	0.026	0.001
U_{r1}	Reaction rate 1	1±0.05	0.001	0.000
U_{r2}	Reaction rate 2	1±0.05	**-0.404**	**0.163**
U_{r3}	Reaction rate 3	1±0.05	0.077	0.006
U_{r4}	Reaction rate 4	1±0.05	**-0.160**	**0.026**
$U_{\rho bo}$	Initial bulk density	1±0.02	-0.075	0.006
U_{To}	Initial temperature	1±0.011	0.078	0.006
$U_{\Sigma niki}$	Avg. BKWS covolume	1±0.01	0.018	0.000
U_{Vswell}	Swell volume	1±0.10	-0.047	0.002
$U_{\omega h2oa}$	Initial adsorbed water	1±0.75	**-0.438**	**0.192**

*This is an uncertainty range.

[a]This is Pearson's correlation coefficient.

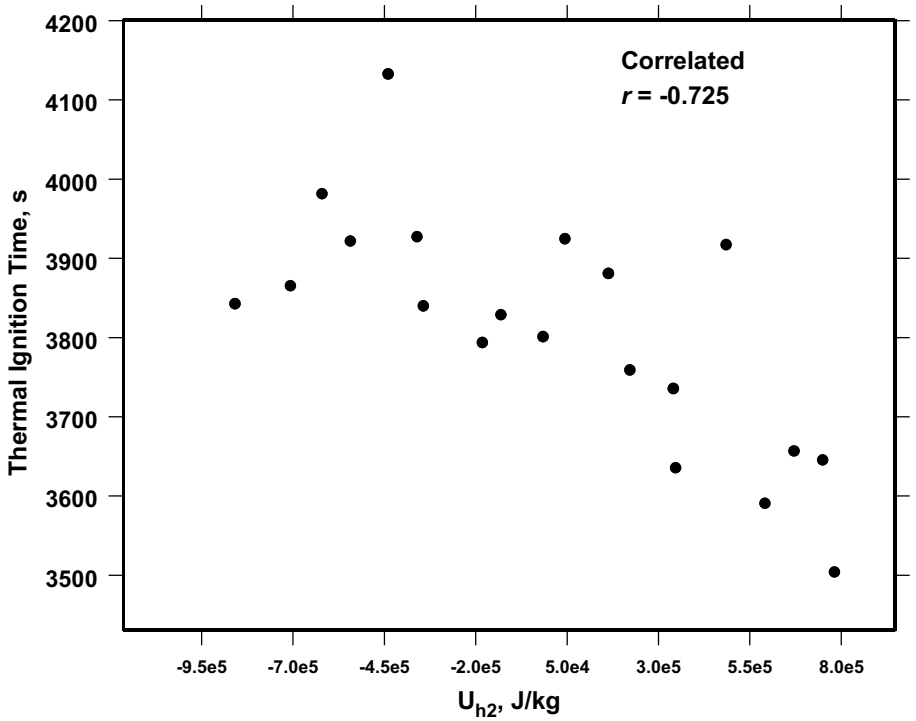

Figure 21. Random variation of the thermal ignition time with the enthalpy of reaction 2, U_{h2}. LHS for SITI experiment 874.

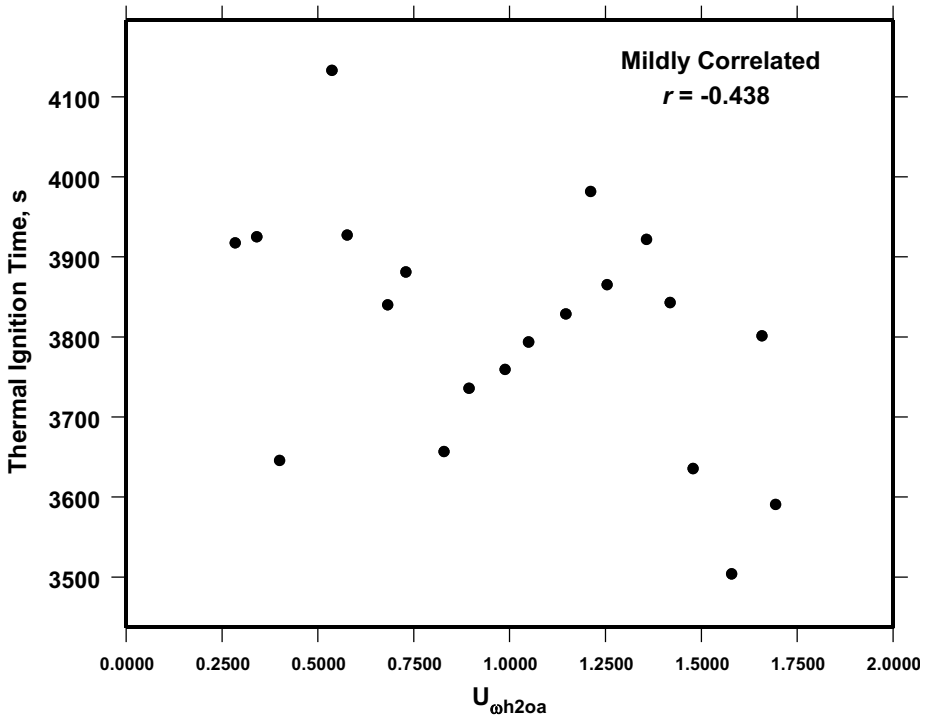

Figure 22. Random variation of the thermal ignition time with the uncertainty multiplier of the initial mass fraction of adsorbed water, $U_{\omega h2oa}$. LHS for SITI experiment 874.

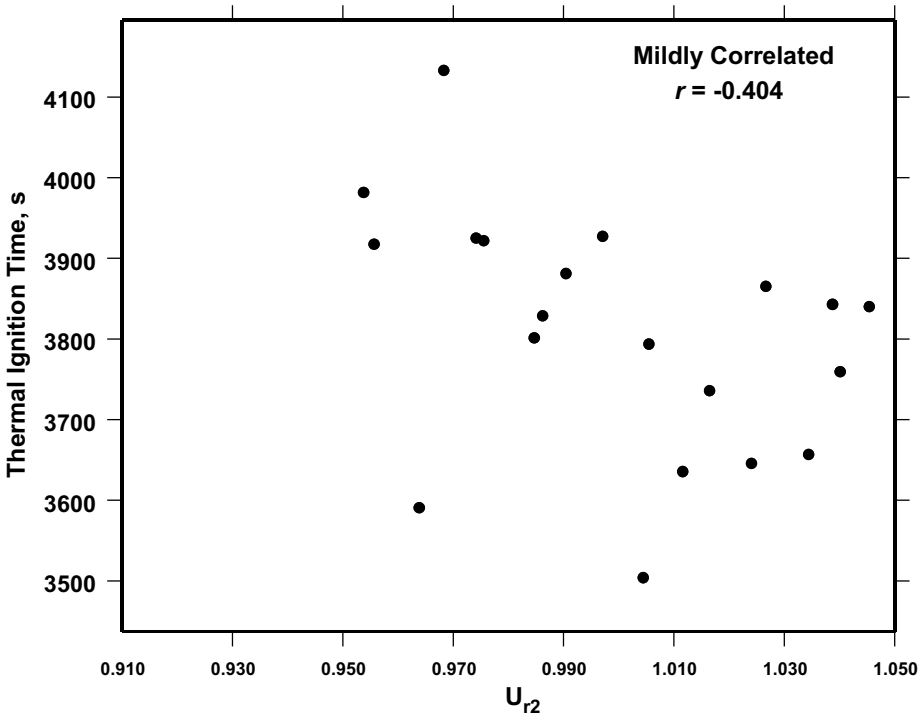

Figure 23. Random variation of the thermal ignition time with the reaction rate 2 uncertainty multiplier, U_{r2}. LHS for SITI experiment 874.

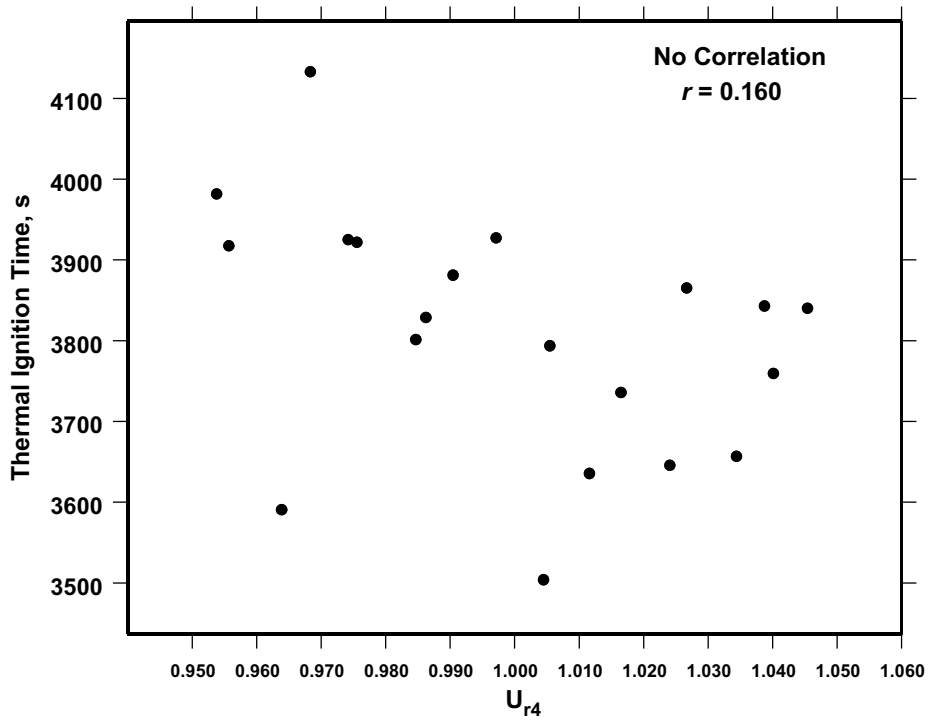

Figure 24. Random variation of the thermal ignition time with the reaction rate 4 uncertainty multiplier, U_{r4}. LHS for SITI experiment 874.

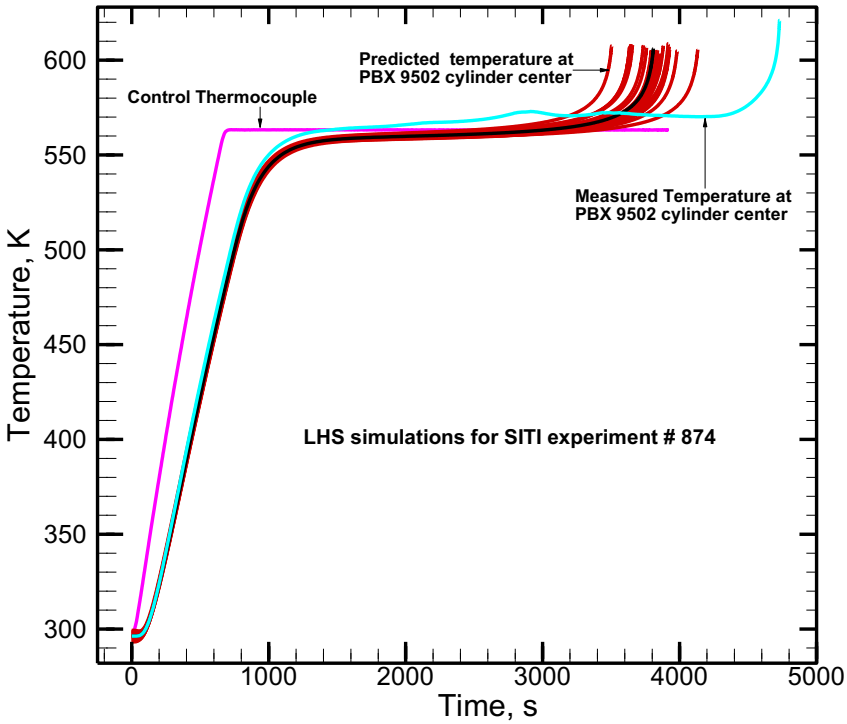

Figure 25. Predicted temperatures for the 20 LHS carried out on SITI experiment 874. The predicted mean center temperature is given in black.

decreases. Figure 21 plots the time to thermal ignition against the enthalpy of reaction 2 for SITI experiment 874. The uncertainty multiplier $U_{\omega h2oa}$ had a correlation coefficient of -0.438. Figure 22 plots the time to thermal ignition against the uncertainty multiplier of the initial mass fraction of water, $U_{\omega h2oa}$. This plot shows that this parameter is mildly correlated. The uncertainty multiplier of reaction rate 2 had a correlation coefficient of -0.404 which implies that as the reaction rate 2 increases, the thermal ignition time decreases. Figure 23 plots this random variation which is mildly correlated. The uncertainty multiplier for reaction rate 4, U_{r4}, had a correlation coefficient of 0.160. Figure 24 shows the plot of the thermal ignition time against U_{r4}. This plot shows that there is no correlation for U_{r4}. Figure 25 shows the temperature results for the 20 LHS for the SITI # 874 experiment. This figure also shows the measured and predicted temperatures at the center of the PBX 9502 cylinder, and thermocouple readings of the boundary condition on the lateral surface of the SITI aluminum confinement. The predicted mean of the temperature at the PBX 9502 cylinder is shown in black.

The third LHS sampling study was done on the experiment SITI # 875 using model option 4 as shown in Table 3. Table 7 shows the results that include the Pearson's correlation coefficient for the thermal ignition time. The uncertainty multiplier of the initial mass fraction of adsorbed water, $U_{\omega h2oa}$, had the highest correlation with a value of -0.600. The sign of this multiplier implies that as $U_{\omega h2oa}$ increases the thermal ignition time decreases. Figure 26 plots the time to thermal ignition against $U_{\omega h2oa}$ for SITI experiment 875. The enthalpy of reaction 2, U_{h2}, had a correlation with a value of -0.517. The sign of this range implies that as U_{h2} increases the thermal ignition time decreases. Figure 27 plots the time to thermal ignition against the enthalpy of reaction 2 for SITI experiment 875. The reaction rate 2 had a correlation coefficient of -0.463 which implies that as

Table 7. Uncertainty multipliers and correlation coefficients for SITI # 875. The most correlated parameters are associated with the uncertainty multipliers $U_{\omega h2oa}$, U_{r2}, U_{r4}, and the range of the enthalpy of reaction 2, U_{h2}.

Symbols	Description	Value	r[a]	r^2
$U_{\beta V}$	Volumetric expansion	1±0.03	-0.137	0.019
U_{Cb}	Bulk specific heat	1±0.05	0.063	0.004
U_{h1}	Reaction 1 enthalpy	1±0.01	0.008	0.000
U_{h2}	Reaction 2 enthalpy*	0±8.6e5	**-0.517**	**0.267**
U_{h3}	Reaction 3 enthalpy	1±0.01	0.118	0.014
U_{h4}	Reaction 4 enthalpy	1±0.01	-0.075	0.006
U_{k}	Thermal conductivity	1±0.05	0.015	0.000
U_{Po}	Initial Pressure	1±0.01	0.023	0.001
U_{r1}	Reaction rate 1	1±0.05	0.024	0.001
U_{r2}	Reaction rate 2	1±0.05	**-0.463**	**0.214**
U_{r3}	Reaction rate 3	1±0.05	0.089	0.008
U_{r4}	Reaction rate 4	1±0.05	**-0.250**	**0.062**
$U_{\rho bo}$	Initial bulk density	1±0.02	-0.065	0.004
U_{To}	Initial temperature	1±0.011	0.020	0.000
$U_{\Sigma niki}$	Avg. BKWS covolume	1±0.01	0.023	0.001
U_{Vswell}	Swell volume	1±0.10	-0.011	0.000
$U_{\omega h2oa}$	Initial adsorbed water	1±0.75	**-0.600**	**0.360**

*This is an uncertainty range.

[a]This is Pearson's correlation coefficient.

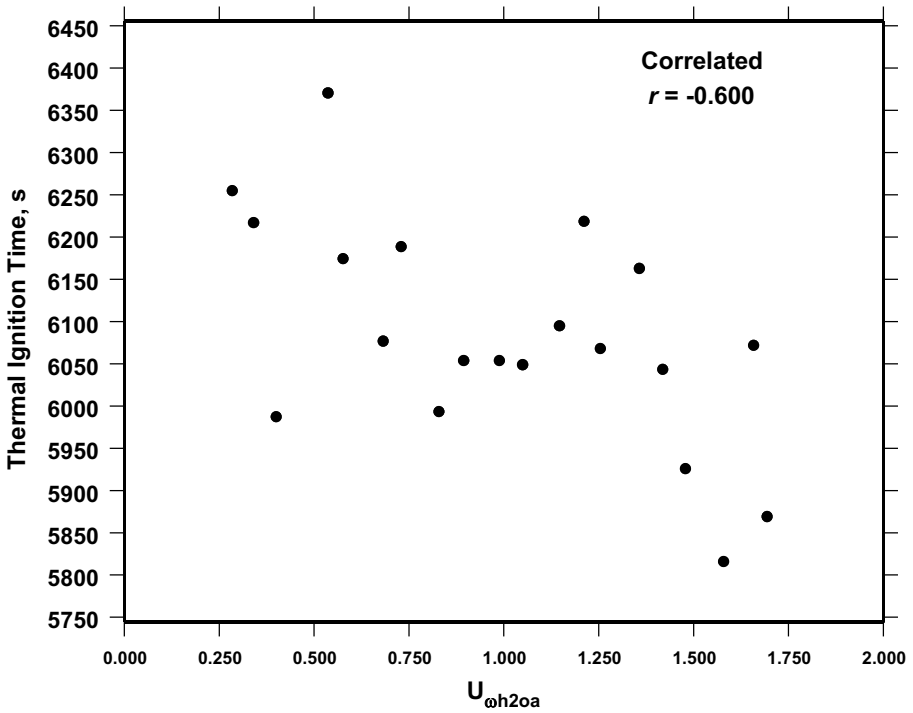

Figure 26. Random variation of the thermal ignition time with the uncertainty multiplier of the initial mass fraction of adsorbed water, $U_{\omega h2oa}$. LHS for SITI experiment 875.

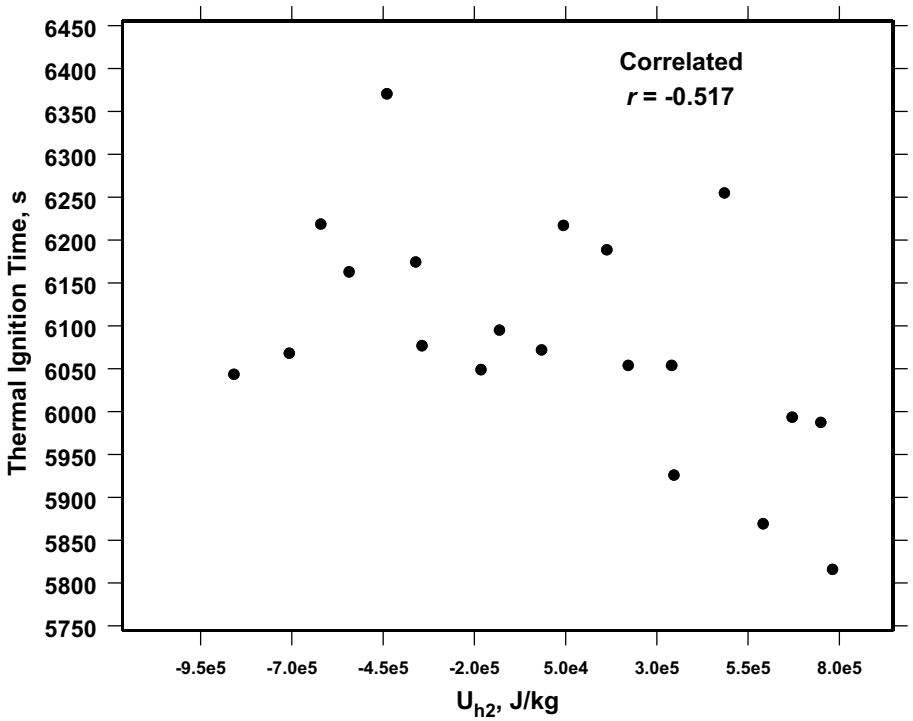

Figure 27. Random variation of the thermal ignition time with the enthalpy of reaction 2, U_{h2}. LHS for SITI experiment 875.

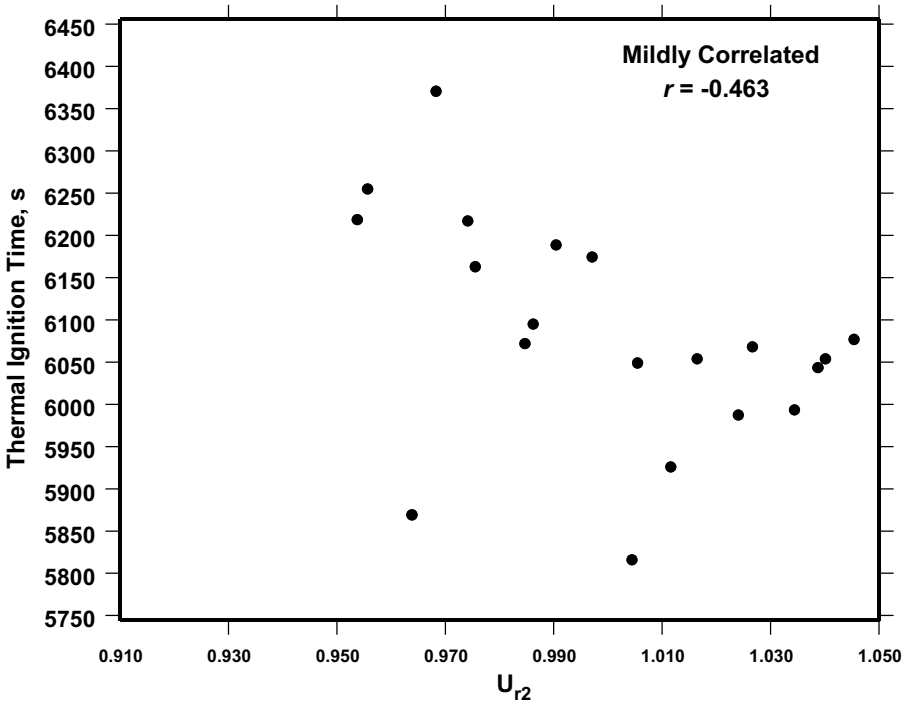

Figure 28. Random variation of the thermal ignition time with the reaction rate 2 uncertainty multiplier, U_{r2}. LHS for SITI experiment 875.

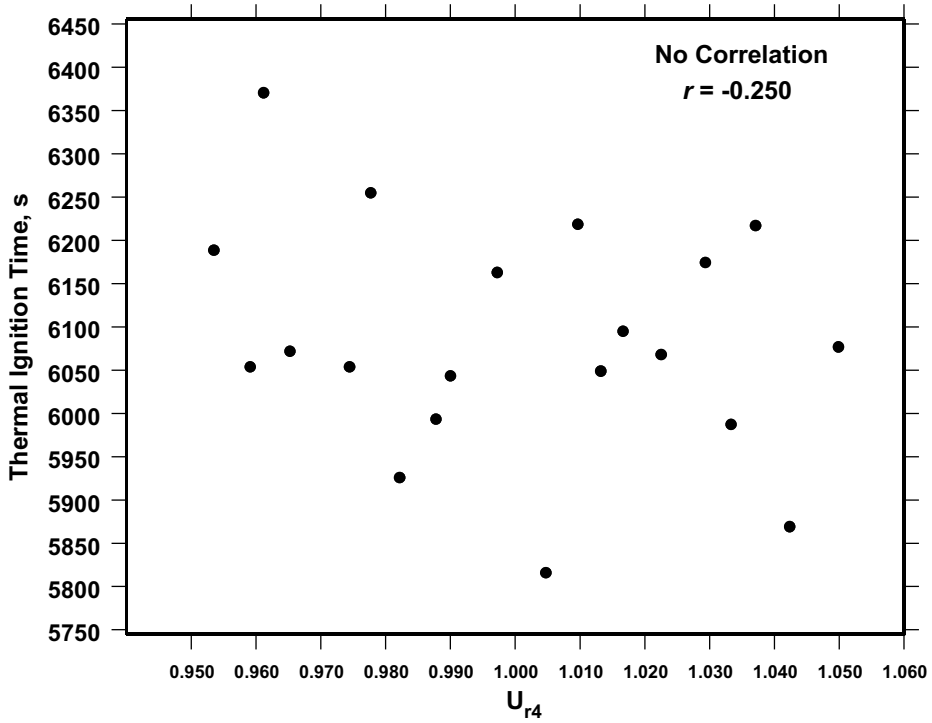

Figure 29. Random variation of the thermal ignition time with the reaction rate 4 uncertainty multiplier, U_{r4}. LHS for SITI experiment 875.

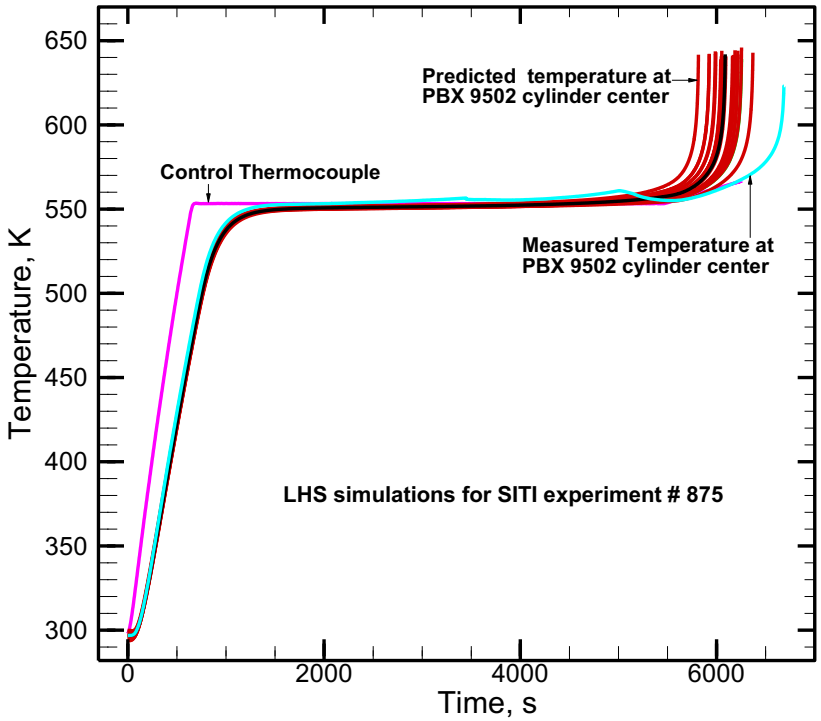

Figure 30. Predicted temperatures for the 20 LHS carried out on SITI experiment 875. The predicted mean center temperature is given in black.

the reaction rate 2 increases, the thermal ignition time decreases. Figure 28 plots this random variation which is mildly correlated. The uncertainty multiplier of reaction rate 4, U_{r4}, had a correlation coefficient of -0.250. Figure 29 shows the plot of the thermal ignition time against U_{r4}. This plot shows that there is no correlation for U_{r4}. Figure 30 shows the temperature results for the 20 LHS for the SITI # 875 experiment. This figure also shows the measured and predicted temperatures at the center of the PBX 9502 cylinder, and thermocouple readings of the boundary condition on the lateral surface of the SITI aluminum confinement. The predicted mean of the temperature at the PBX 9502 cylinder is shown in black.

The fourth LHS sampling study was done on the experiment SITI # 876 using model option 3 as shown in Table 3. Table 8 shows the results that include the Pearson's correlation coefficient for the thermal ignition time. The uncertainty multiplier $U_{\omega h2oa}$ had the highest correlation with a value of -0.712. The sign of this multiplier implies that as the initial adsorbed water mass fraction increases, the time to thermal ignition decreases. Figure 31 plots the time to thermal ignition against $U_{\omega h2oa}$. The swell volume had a correlation coefficient of 0.472 which implies that as the swell volume increases, the thermal ignition time increases. Figure 32 plots the random variation of the thermal ignition time with the swell volume uncertainty multiplier. The reaction rate 2 had a correlation coefficient of -0.444 which implies that as the reaction rate 2 increases, the thermal ignition time decreases. Figure 33 plots the random variation of the thermal ignition time with the reaction rate 2 uncertainty multiplier. The uncertainty multiplier for reaction rate 4, U_{r4}, had a correlation coefficient of -0.244. Figure 34 shows the plot of the thermal ignition time against U_{r4}. Figure 34 shows almost no correlation for the uncertainty multiplier U_{r4}. The uncertainty multiplier for reaction rate 4, U_{r4}, had a correlation coefficient of -0.244. Figure 19 shows the plot of the thermal ignition time against U_{r4}. Figure 34 shows almost no correlation for the uncertainty

Table 8. Uncertainty multipliers and correlation coefficients for SITI # 876. The most correlated parameters are associated with the uncertainty multipliers $U_{\omega h2oa}$, U_{Vswell}, U_{r2}, and U_{r4}.

Symbols	Description	Value	r^a	r^2
$U_{\beta V}$	Volumetric expansion	1±0.03	-0.120	0.014
U_{Cb}	Bulk specific heat	1±0.05	-0.014	0.000
U_{h1}	Reaction 1 enthalpy	1±0.01	0.016	0.000
U_{h2}	Reaction 2 enthalpy*	0±8.6e5	-0.008	0.000
U_{h3}	Reaction 3 enthalpy	1±0.01	0.185	0.034
U_{h4}	Reaction 4 enthalpy	1±0.01	0.002	0.000
U_{k}	Thermal conductivity	1±0.05	-0.014	0.000
U_{Po}	Initial Pressure	1±0.01	0.033	0.001
U_{r1}	Reaction rate 1	1±0.05	0.068	0.005
U_{r2}	Reaction rate 2	1±0.05	**-0.444**	**0.197**
U_{r3}	Reaction rate 3	1±0.05	0.003	0.000
U_{r4}	Reaction rate 4	1±0.05	**-0.244**	**0.059**
$U_{\rho bo}$	Initial bulk density	1±0.02	-0.067	0.004
U_{To}	Initial temperature	1±0.011	-0.030	0.001
$U_{\Sigma niki}$	Avg. BKWS covolume	1±0.01	0.014	0.000
U_{Vswell}	Swell volume	1±0.10	**0.472**	**0.223**
$U_{\omega h2oa}$	Initial adsorbed water	1±0.75	**-0.712**	**0.506**

*This is an uncertainty range.

[a]This is Pearson's correlation coefficient.

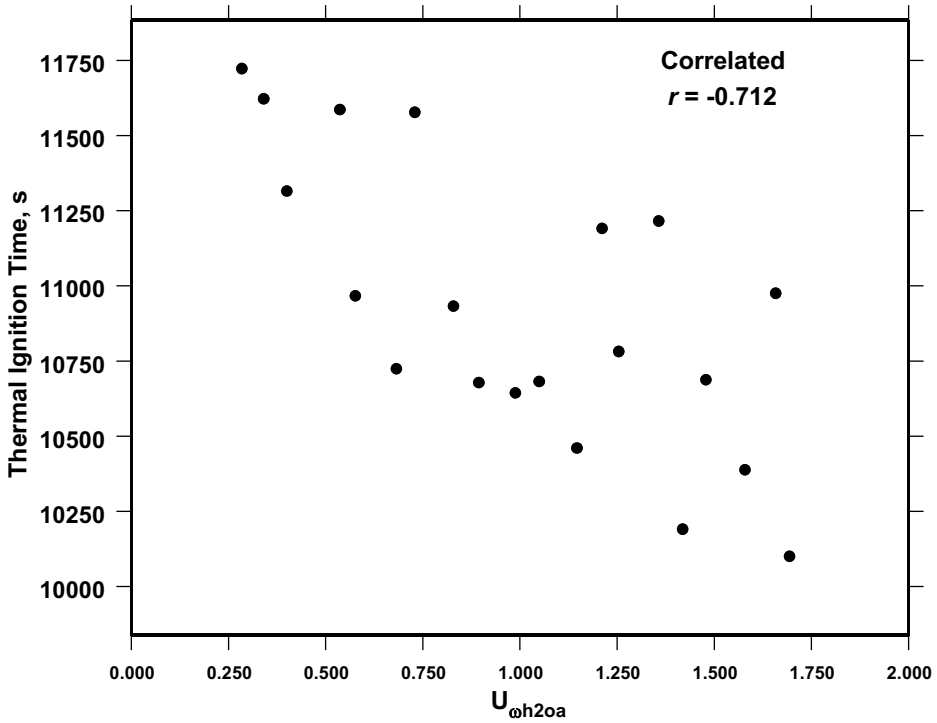

Figure 31. Random variation of the thermal ignition time with the uncertainty multiplier of the initial mass fraction of adsorbed water, $U_{\omega h2oa}$. LHS for SITI experiment 876.

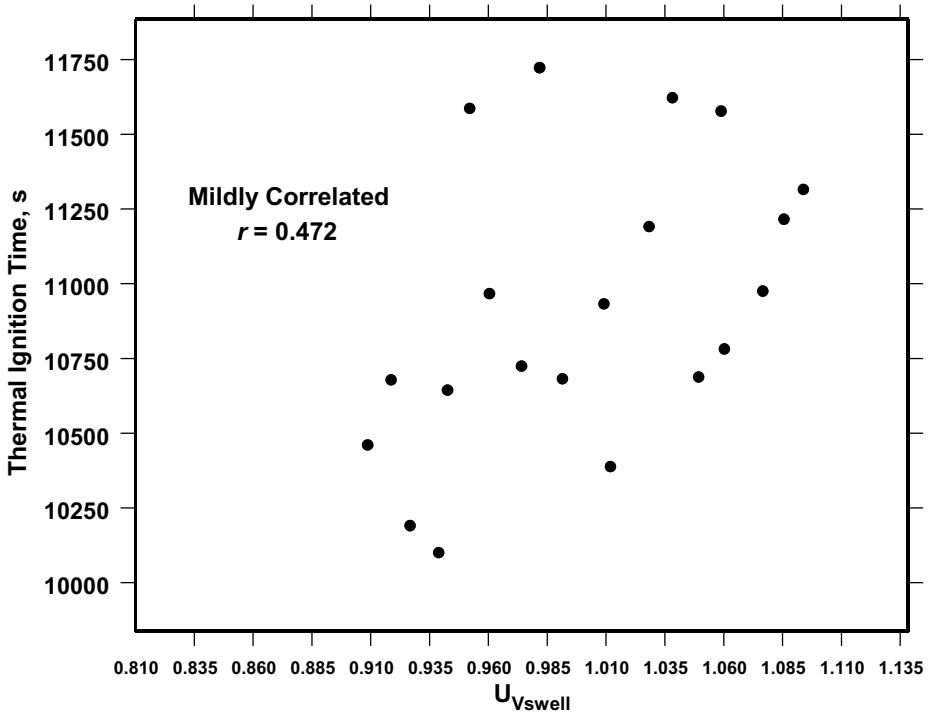

Figure 32. Random variation of the thermal ignition time with the swell volume uncertainty multiplier, U_{Vswell}. LHS for SITI experiment 876.

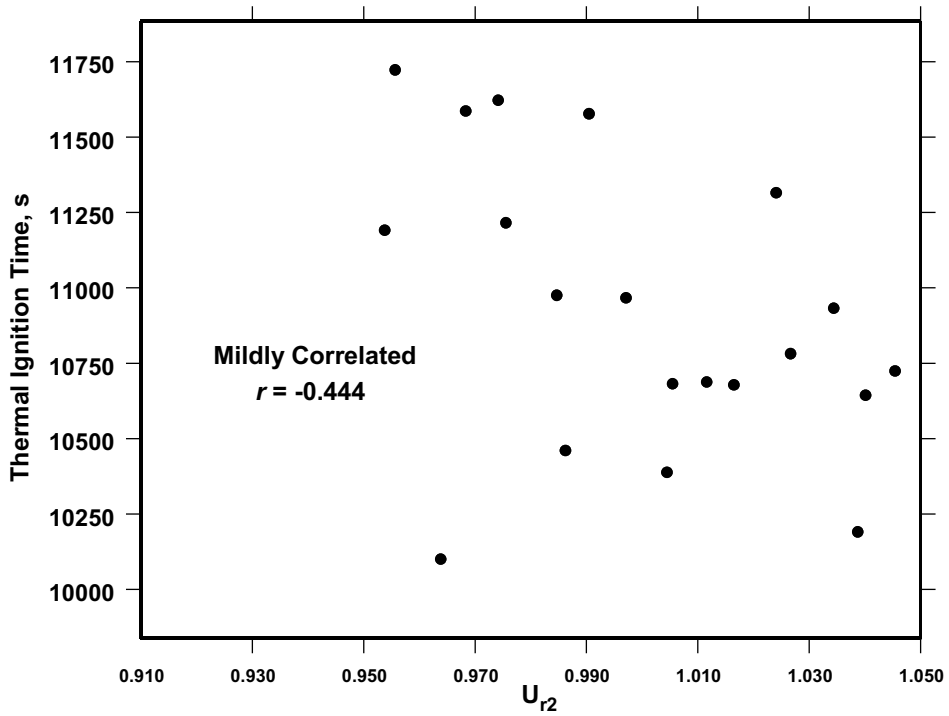

Figure 33. Random variation of the thermal ignition time with the reaction rate 2 uncertainty multiplier, U_{r2}. LHS for SITI experiment 876.

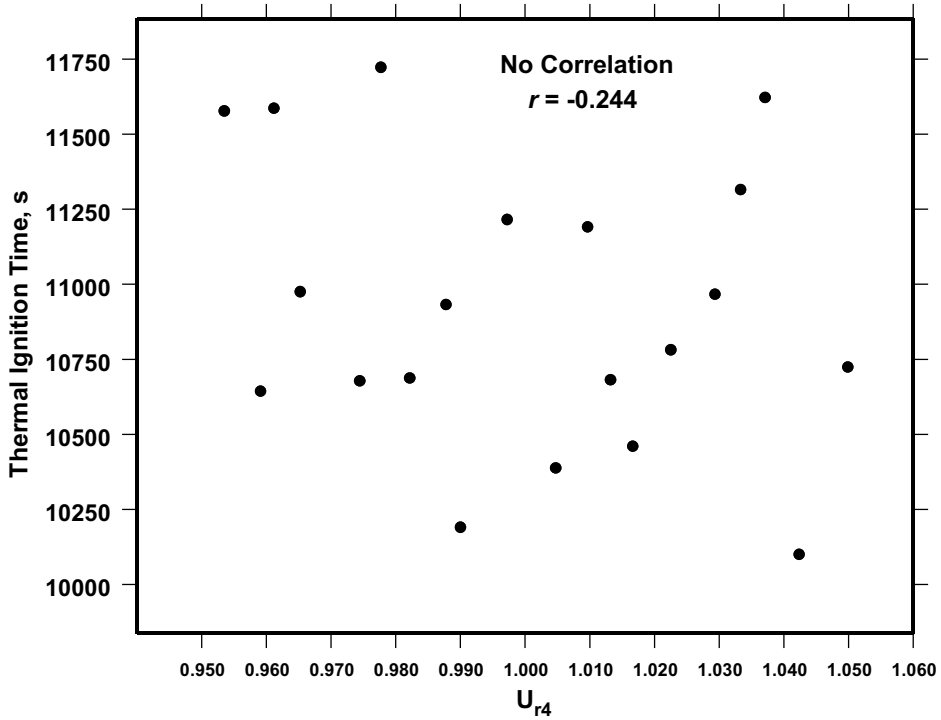

Figure 34. Random variation of the thermal ignition time with the reaction rate 4 uncertainty multiplier, U_{r4}. LHS for SITI experiment 876.

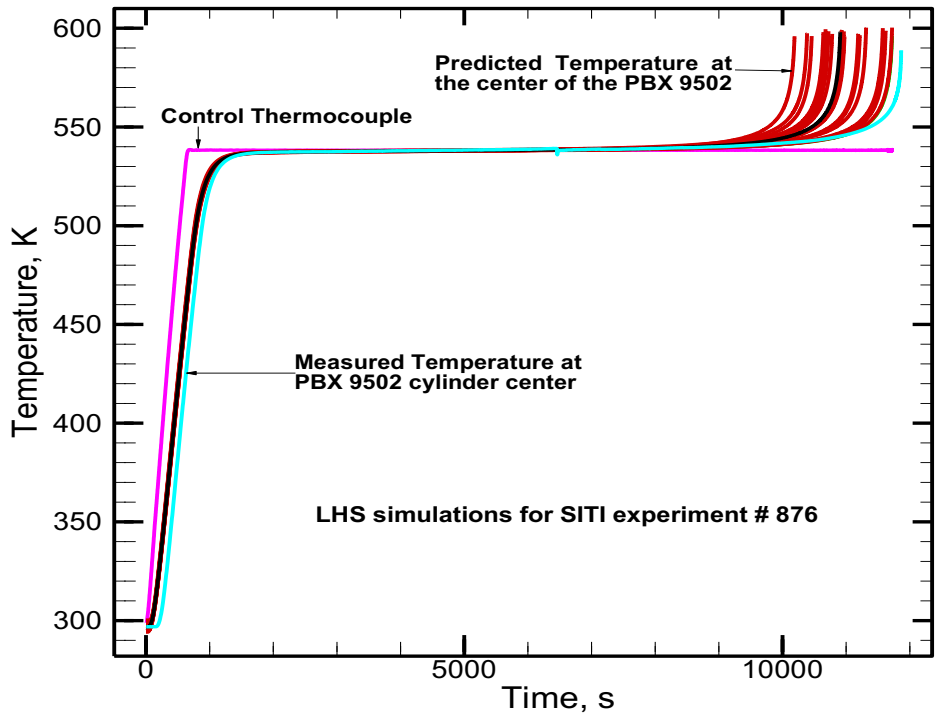

Figure 35. Predicted temperatures for the 20 LHS carried out on the SITI experiment 876. The predicted mean center temperature is given in black.

multiplier U_{r4}. Figure 35 shows the temperature results for the 20 LHS for the SITI # 876 experiment. This figure also shows the measured and predicted temperatures at the center of the PBX 9502 cylinder, and thermocouple readings of the boundary condition on the lateral surface of the SITI aluminum confinement. The predicted mean of the temperature at the PBX 9502 cylinder is shown in black.

The fifth LHS sampling study was done on the experiment SITI # 877 using model option 4 as shown in Table 3. Table 9 shows the results that include the Pearson's correlation coefficient for the thermal ignition time. The uncertainty multiplier of the initial mass fraction of adsorbed water, $U_{\omega h2oa}$, had the highest correlation with a value of -0.617. The sign of this multiplier implies that as $U_{\omega h2oa}$ increases the thermal ignition time decreases. Figure 36 plots the time to thermal ignition against $U_{\omega h2oa}$ for SITI experiment 877. The enthalpy of reaction 2, U_{h2}, had a correlation with a value of -0.531. The sign of this range implies that as U_{h2} increases the thermal ignition time decreases. Figure 37 plots the time to thermal ignition against the enthalpy of reaction 2 for SITI experiment 877. The reaction rate 2 had a correlation coefficient of -0.441 which implies that as the reaction rate 2 increases, the thermal ignition time decreases. Figure 38 plots this random variation which is mildly correlated. The uncertainty multiplier of reaction rate 4, U_{r4}, had a correlation coefficient of -0.199. Figure 39 shows the plot of the thermal ignition time against U_{r4}. This plot shows that there is no correlation for U_{r4}. Figure 40 shows the temperature results for the 20 LHS for the SITI # 877 experiment. This figure also shows the measured and predicted temperatures at the center of the PBX 9502 cylinder, and thermocouple readings of the boundary condition on the lateral surface of the SITI aluminum confinement. The predicted mean of the temperature at the PBX 9502 cylinder is shown in black.

The sixth LHS sampling study was done on the experiment SITI # 878 using model option 2 as shown in Table 3. Table 10 shows the results that include the Pearson's correlation coefficient for

Table 9. Uncertainty multipliers and correlation coefficients for SITI # 877. The most correlated parameters are associated with the uncertainty multipliers $U_{\omega h2oa}$, U_{r2}, U_{r4}, and the range of the enthalpy of reaction 2, U_{h2}.

Symbols	Description	Value	r^a	r^2
$U_{\beta V}$	Volumetric expansion	1±0.03	-0.154	0.024
U_{Cb}	Bulk specific heat	1±0.05	0.104	0.011
U_{h1}	Reaction 1 enthalpy	1±0.01	0.004	0.000
U_{h2}	Reaction 2 enthalpy*	0±8.6e5	**-0.531**	**0.282**
U_{h3}	Reaction 3 enthalpy	1±0.01	0.135	0.018
U_{h4}	Reaction 4 enthalpy	1±0.01	-0.062	0.004
U_k	Thermal conductivity	1±0.05	-0.008	0.000
U_{Po}	Initial Pressure	1±0.01	0.028	0.001
U_{r1}	Reaction rate 1	1±0.05	-0.010	0.000
U_{r2}	Reaction rate 2	1±0.05	**-0.441**	**0.194**
U_{r3}	Reaction rate 3	1±0.05	0.075	0.006
U_{r4}	Reaction rate 4	1±0.05	**-0.199**	**0.040**
$U_{\rho bo}$	Initial bulk density	1±0.02	-0.061	0.004
U_{To}	Initial temperature	1±0.011	0.053	0.003
$U_{\Sigma niki}$	Avg. BKWS covolume	1±0.01	-0.005	0.000
U_{Vswell}	Swell volume	1±0.10	-0.032	0.001
$U_{\omega h2oa}$	Initial adsorbed water	1±0.75	**-0.617**	**0.381**

*This is an uncertainty range.

[a]This is Pearson's correlation coefficient.

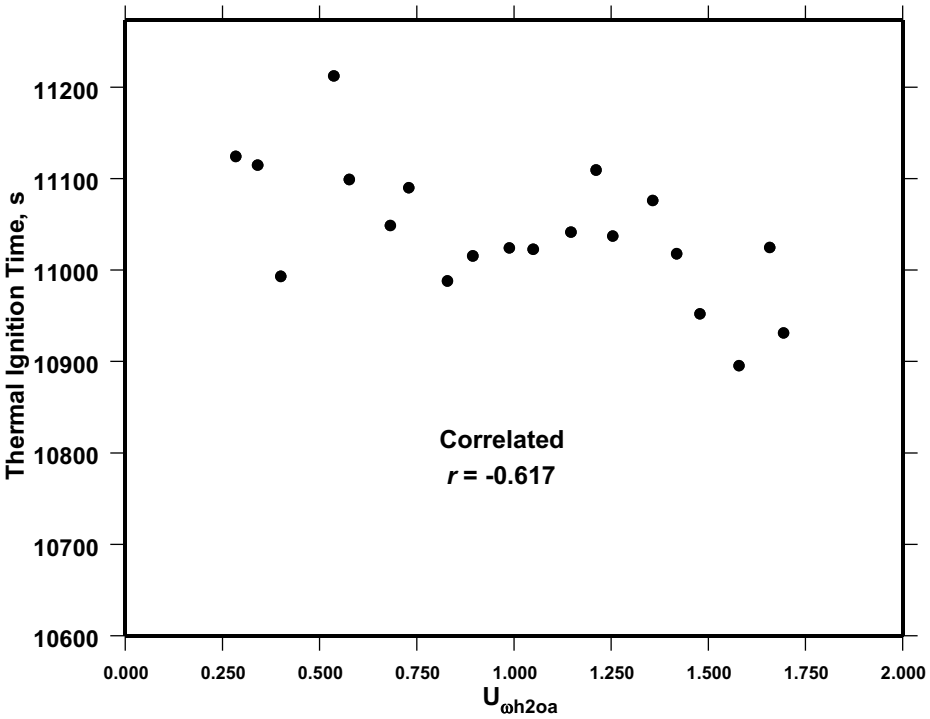

Figure 36. Random variation of the thermal ignition time with the uncertainty multiplier of the initial mass fraction of adsorbed water, $U_{\omega h2oa}$. LHS for SITI experiment 877.

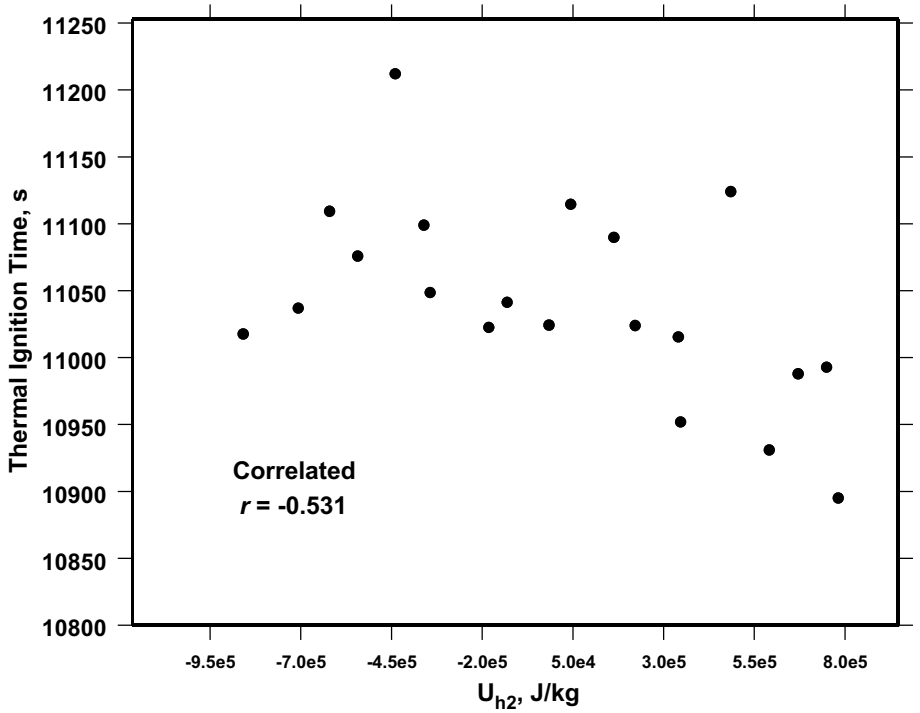

Figure 37. Random variation of the thermal ignition time with the enthalpy of reaction 2, U_{h2}. LHS for SITI experiment 877.

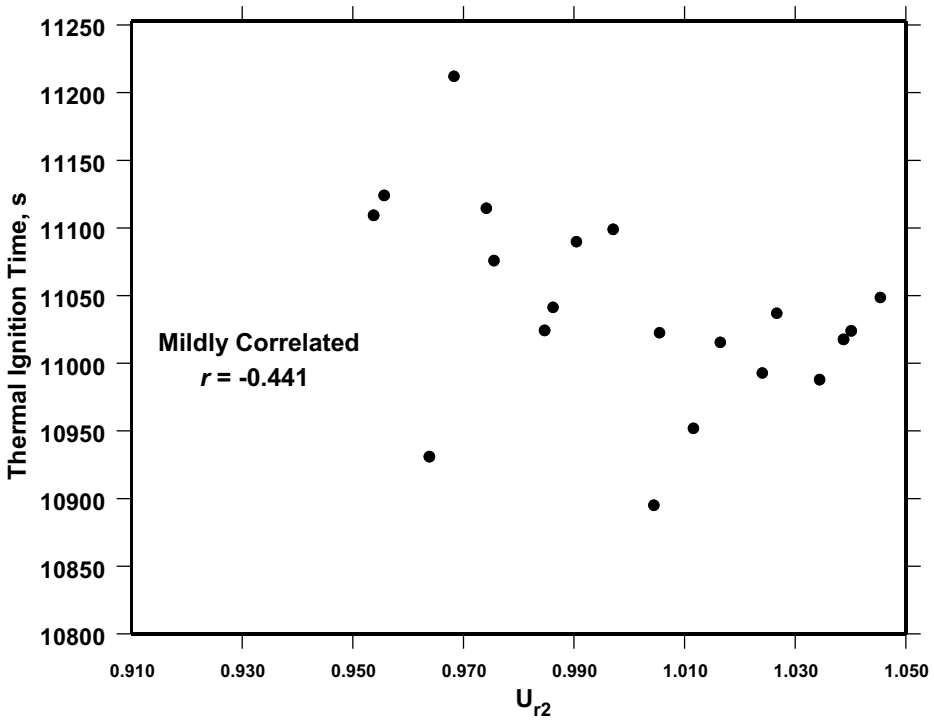

Figure 38. Random variation of the thermal ignition time with the reaction rate 2 uncertainty multiplier, U_{r2}. LHS for SITI experiment 877.

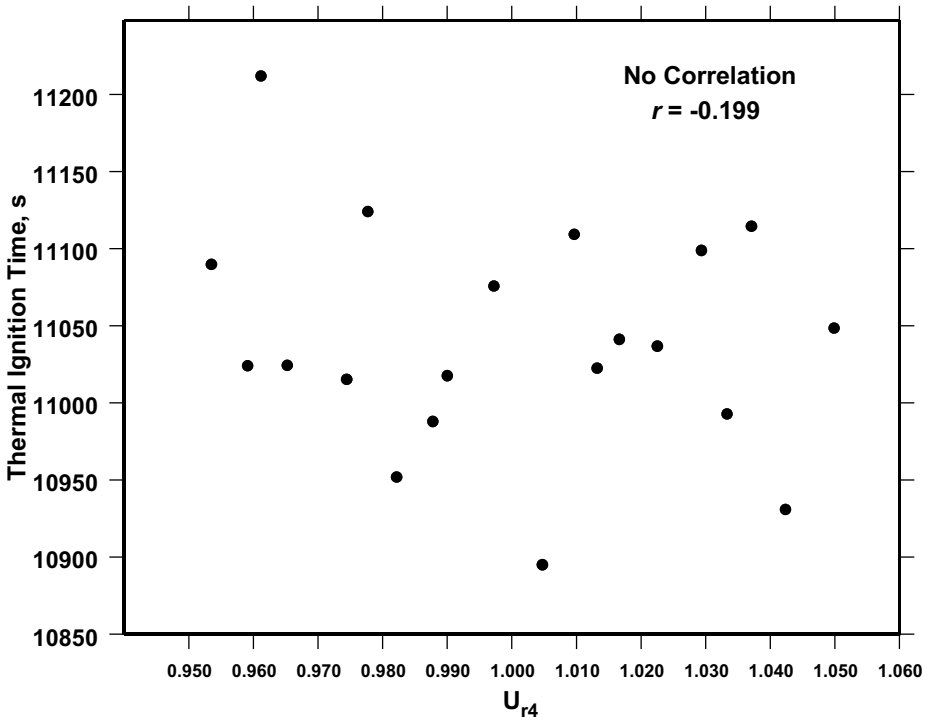

Figure 39. Random variation of the thermal ignition time with the reaction rate 4 uncertainty multiplier, U_{r4}. LHS for SITI experiment 877.

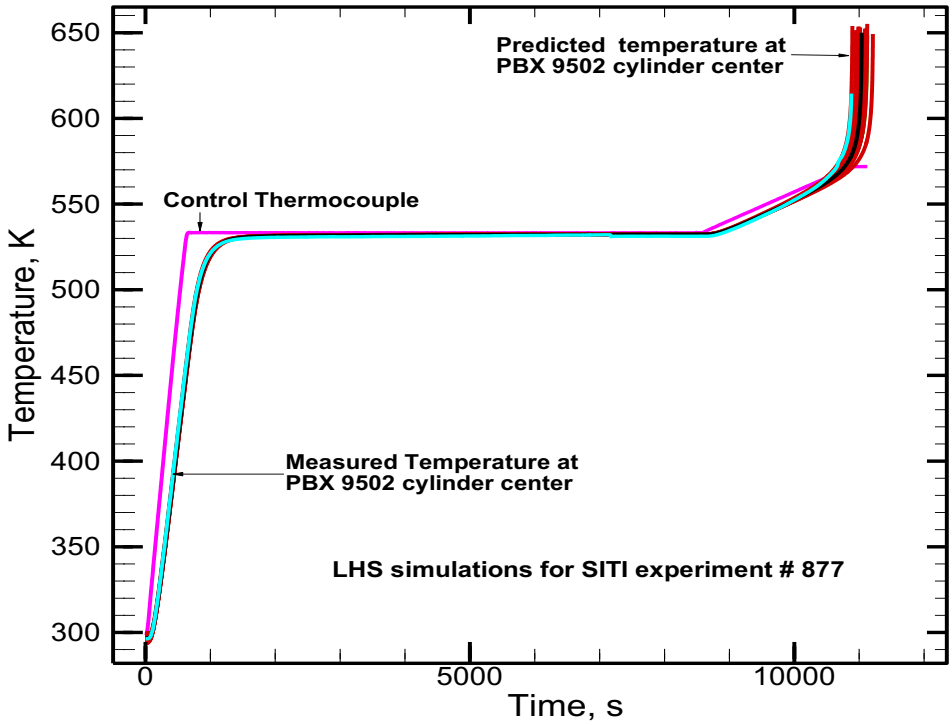

Figure 40. Predicted temperatures for the 20 LHS carried out on SITI experiment 877. The predicted mean center temperature is given in black.

the thermal ignition time. The uncertainty multiplier of the initial mass fraction of adsorbed water, $U_{\omega h2oa}$, had the highest correlation with a value of -0.710. The sign of this multiplier implies that as $U_{\omega h2oa}$ increases the thermal ignition time decreases. Figure 41 plots the time to thermal ignition against $U_{\omega h2oa}$ for SITI experiment 878. The reaction rate 2 had a correlation coefficient of -0.411 which implies that as the reaction rate 2 increases, the thermal ignition time decreases. Figure 42 plots this random variation which is mildly correlated. The uncertainty multiplier for the swell volume had a correlation coefficient of 0.397. Figure 43 plots the thermal ignition time against U_{Vswell}. Figure 43 shows that U_{Vswell} is mildly correlated. The enthalpy of reaction 2, U_{h2}, had a correlation with a value of -0.242. Figure 44 plots the time to thermal ignition against the enthalpy of reaction 2 for SITI experiment 878. This plot shows that there is no correlation for U_{h2}. Figure 45 shows the temperature results for the 20 LHS for the SITI # 878 experiment. This figure also shows the measured and predicted temperatures at the center of the PBX 9502 cylinder, and thermocouple readings of the boundary condition on the lateral surface of the SITI aluminum confinement. The predicted mean of the temperature at the PBX 9502 cylinder is shown in black.

The seventh LHS sampling study was done on the experiment SITI # 880 using the experimental pressure as shown in Table 3. Table 11 shows the results that include the Pearson's correlation coefficient for the thermal ignition time. The most correlated parameters were the ones associated with the mono-furazan formation reaction 2. This is to be expected because the experimental pressure was fed to the cookoff model. This bypassed all the steps associated with the calculation of the pressure in Eq. (12) and the experimental pressure was substituted directly into the reaction rate equation (10). The number of moles of gases produced by the decomposition, n, the average temperature, T_{ave}, and the volume generated by the decomposition gases, V_g, didn't have any influence on the calculation of the pressure. This is probably why $U_{\omega h2oa}$ wasn't correlated

Table 10. Uncertainty multipliers and correlation coefficients for SITI # 878. The most correlated parameters are associated with the uncertainty multipliers $U_{\omega h2oa}$, U_{r2}, U_{Vswell}, the range of the enthalpy of reaction 2, U_{h2}, and U_{r4}.

Symbols	Description	Value	r^a	r^2
$U_{\beta V}$	Volumetric expansion	1±0.03	-0.128	0.016
U_{Cb}	Bulk specific heat	1±0.05	0.062	0.004
U_{h1}	Reaction 1 enthalpy	1±0.01	-0.006	0.000
U_{h2}	Reaction 2 enthalpy*	0±8.6e5	**-0.242**	**0.059**
U_{h3}	Reaction 3 enthalpy	1±0.01	0.191	0.037
U_{h4}	Reaction 4 enthalpy	1±0.01	-0.030	0.001
U_k	Thermal conductivity	1±0.05	-0.037	0.001
U_{Po}	Initial Pressure	1±0.01	0.013	0.000
U_{r1}	Reaction rate 1	1±0.05	0.040	0.002
U_{r2}	Reaction rate 2	1±0.05	**-0.411**	**0.169**
U_{r3}	Reaction rate 3	1±0.05	0.032	0.001
U_{r4}	Reaction rate 4	1±0.05	**-0.181**	**0.033**
$U_{\rho bo}$	Initial bulk density	1±0.02	-0.099	0.010
U_{To}	Initial temperature	1±0.011	0.000	0.000
$U_{\Sigma niki}$	Avg. BKWS covolume	1±0.01	-0.013	0.000
U_{Vswell}	Swell volume	1±0.10	**0.397**	**0.158**
$U_{\omega h2oa}$	Initial adsorbed water	1±0.75	**-0.710**	**0.505**

*This is an uncertainty range.

[a]This is Pearson's correlation coefficient.

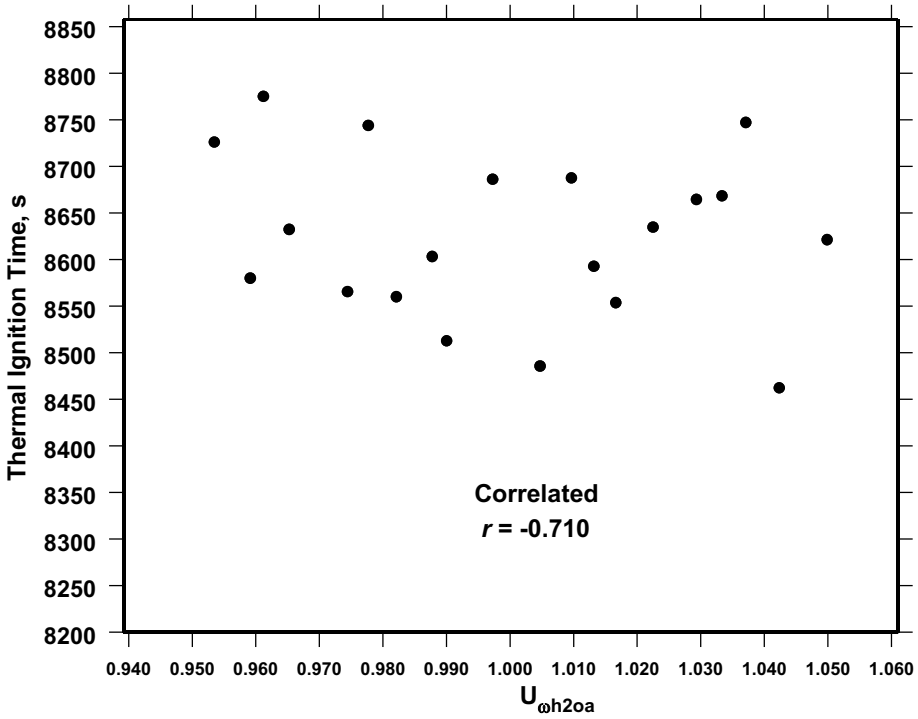

Figure 41. Random variation of the thermal ignition time with the uncertainty multiplier of the initial mass fraction of adsorbed water, $U_{\omega h2oa}$. LHS for SITI experiment 878.

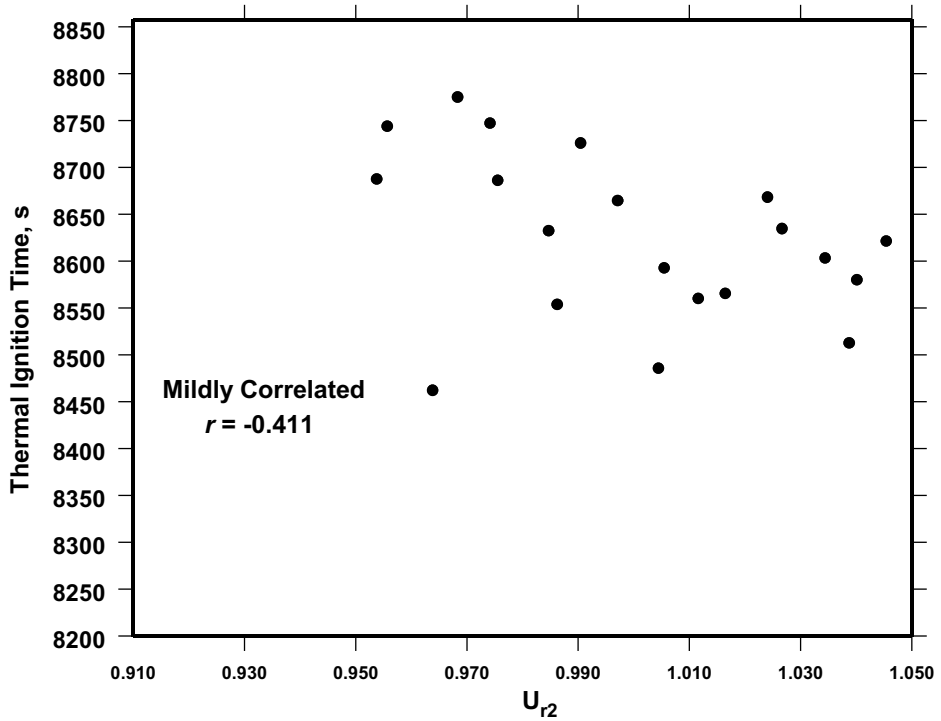

Figure 42. Random variation of the thermal ignition time with the reaction rate 2 uncertainty multiplier, U_{r2}. LHS for SITI experiment 878.

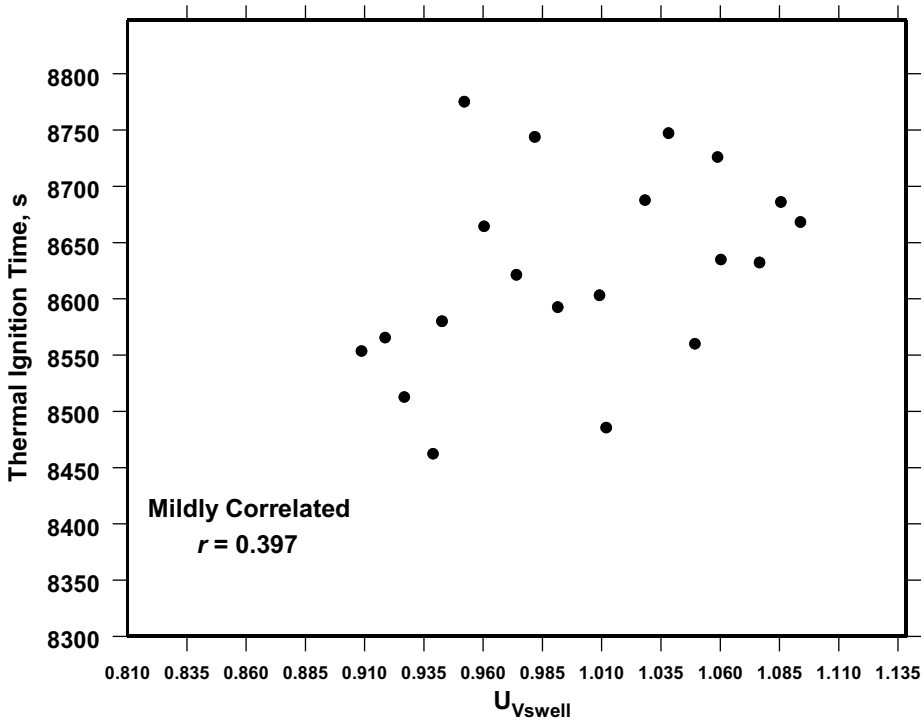

Figure 43. Random variation of the thermal ignition time with the swell volume uncertainty multiplier, U_{Vswell}. LHS for SITI experiment 878.

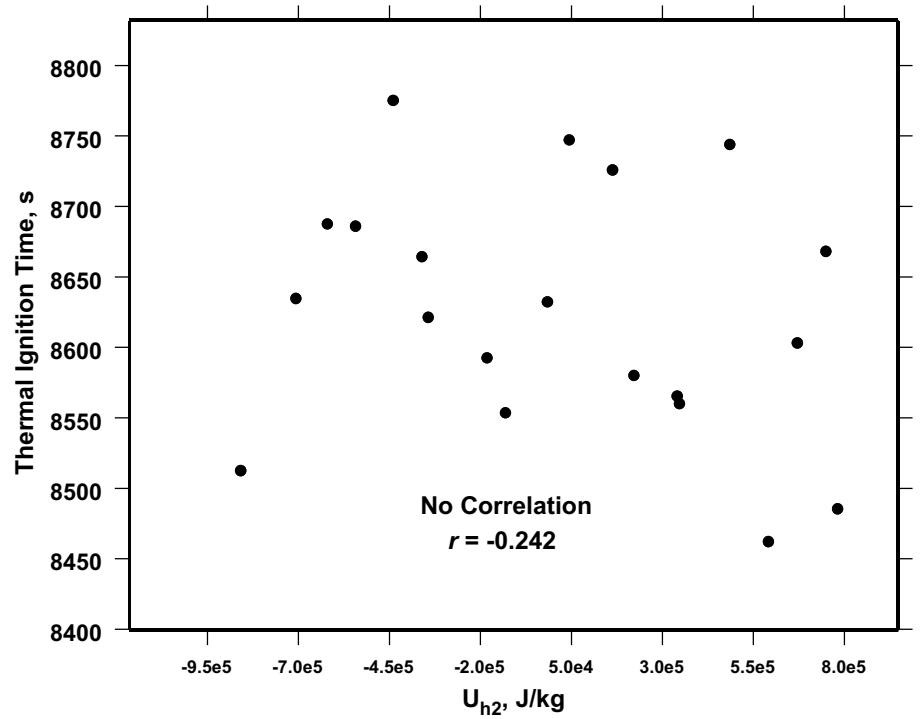

Figure 44. Random variation of the thermal ignition time with the enthalpy of reaction 2, U_{h2}. LHS for SITI experiment 878.

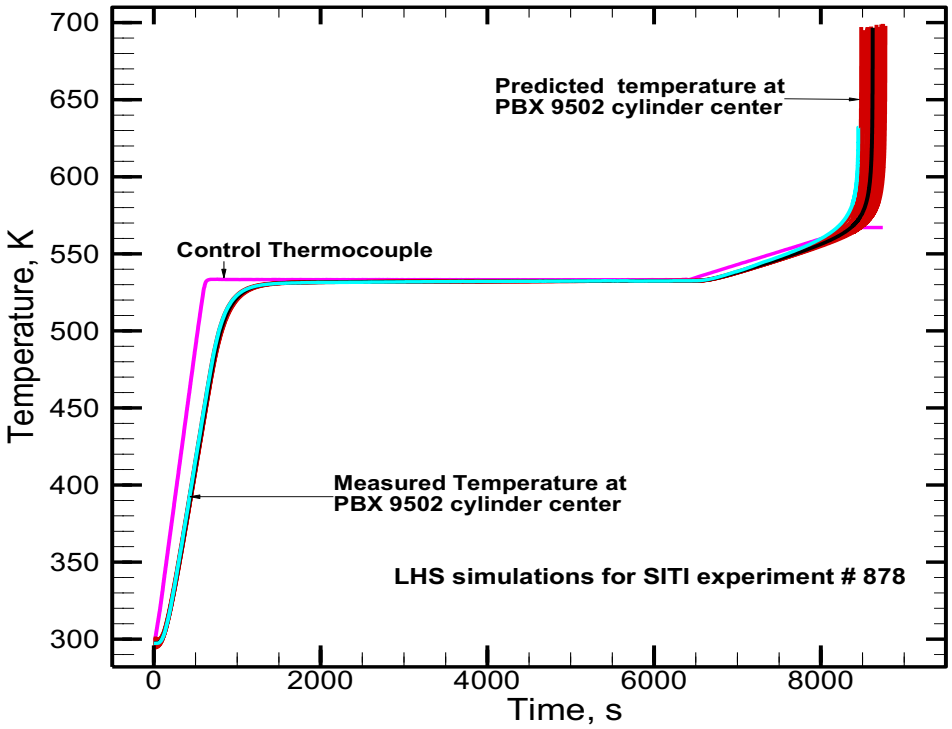

Figure 45. Predicted temperatures for the 20 LHS carried out on SITI experiment 878. The predicted mean center temperature is given in black.

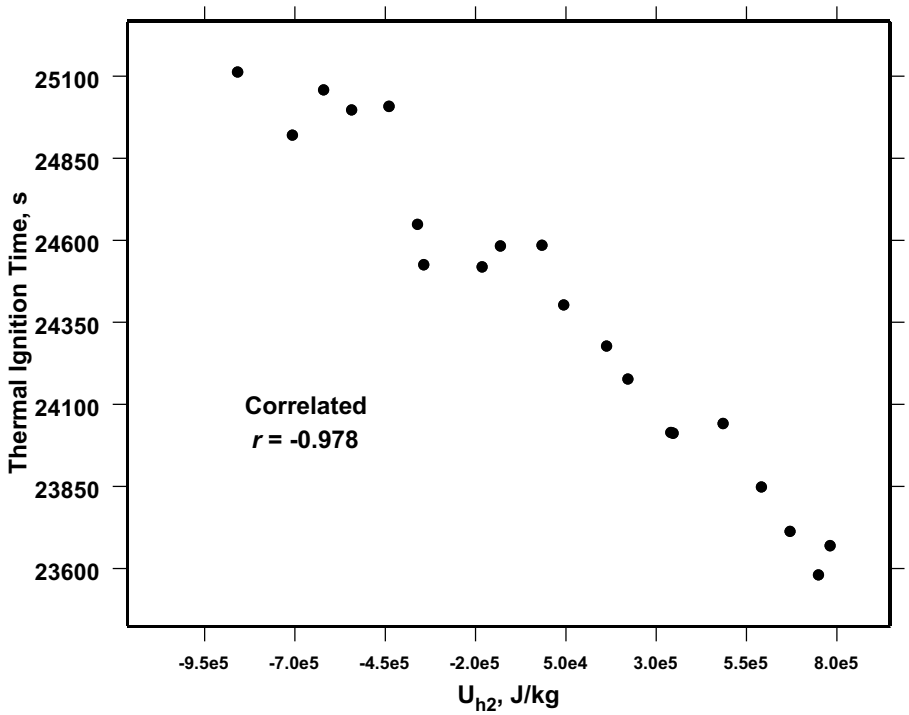

Figure 46. Random variation of the thermal ignition time with the enthalpy of reaction 2, U_{h2}. LHS for SITI experiment 880.

Table 11. Uncertainty multipliers and correlation coefficients for SITI # 880. The most correlated parameters are associated with the range of the enthalpy of reaction 2 and U_{r2}.

Symbols	Description	Value	r^a	r^2
$U_{\beta V}$	Volumetric expansion	1±0.03	-0.080	0.006
U_{Cb}	Bulk specific heat	1±0.05	-0.005	0.000
U_{h1}	Reaction 1 enthalpy	1±0.01	-0.007	0.000
U_{h2}	Reaction 2 enthalpy*	0±8.6e5	**-0.978**	**0.956**
U_{h3}	Reaction 3 enthalpy	1±0.01	0.060	0.004
U_{h4}	Reaction 4 enthalpy	1±0.01	-0.041	0.002
U_k	Thermal conductivity	1±0.05	0.144	0.021
U_{Po}	Initial Pressure	1±0.01	0.023	0.000
U_{r1}	Reaction rate 1	1±0.05	-0.003	0.000
U_{r2}	Reaction rate 2	1±0.05	**-0.191**	**0.036**
U_{r3}	Reaction rate 3	1±0.05	0.069	0.005
U_{r4}	Reaction rate 4	1±0.05	-0.030	0.001
$U_{\rho bo}$	Initial bulk density	1±0.02	-0.084	0.007
U_{To}	Initial temperature	1±0.011	0.128	0.016
$U_{\Sigma niki}$	Avg. BKWS covolume	1±0.01	0.027	0.001
U_{Vswell}	Swell volume	1±0.10	-0.055	0.003
$U_{\omega h2oa}$	Initial adsorbed water	1±0.75	0.110	0.012

*This is an uncertainty range.

[a]This is Pearson's correlation coefficient.

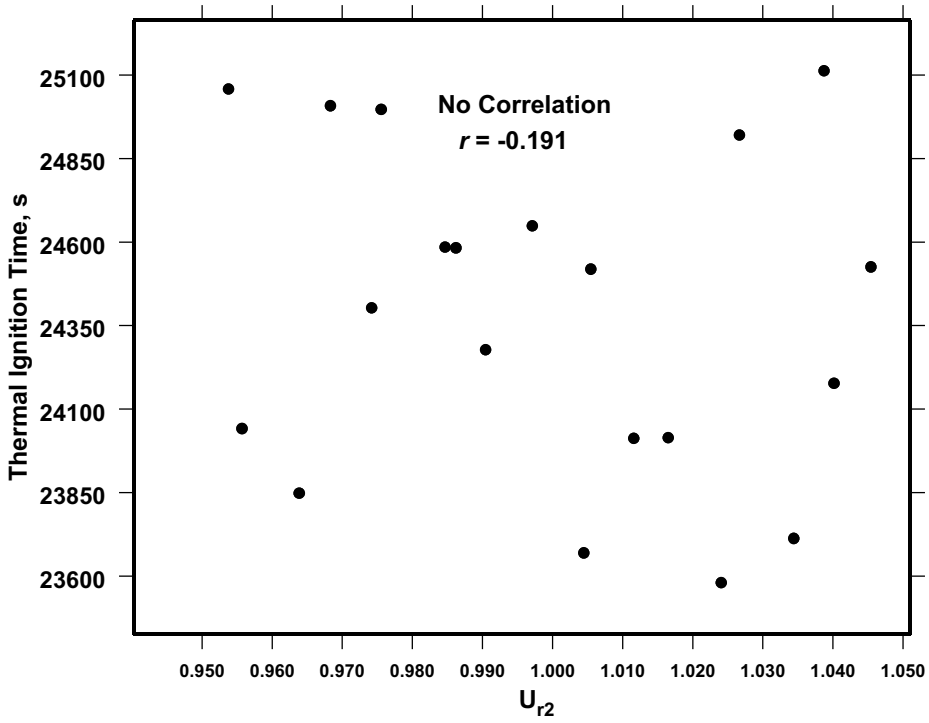

Figure 47. Random variation of the thermal ignition time with the reaction rate 2 uncertainty multiplier, U_{r2}. LHS for SITI experiment 880.

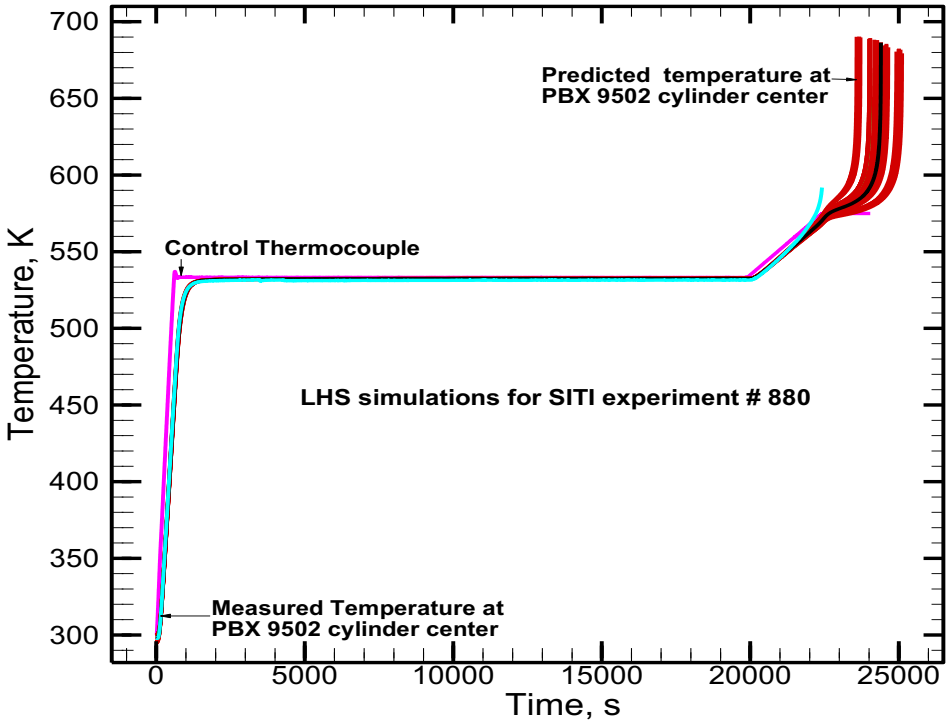

Figure 48. Predicted temperatures for the 20 LHS carried out on SITI experiment 880. The predicted mean center temperature is given in black.

(as shown in Table 11) for this case as it was in some of the previous cases in which the experimental pressure wasn't fed to the cookoff model. Table 11 shows that the enthalpy of reaction 2, U_{h2}, had a correlation with a value of -0.978. Figure 46 plots the time to thermal ignition against the enthalpy of reaction 2 for SITI experiment 880. The reaction rate 2, U_{r2}, had a correlation with a value of -0.191. Figure 47 plots the time to thermal ignition against the reaction rate 2 for SITI experiment 880. This plot shows no correlation for this parameter. Figure 48 shows the temperature results for the 20 LHS for the SITI # 880 experiment. This figure also shows the measured and predicted temperatures at the center of the PBX 9502 cylinder, and thermocouple readings of the boundary condition on the lateral surface of the SITI aluminum confinement. The predicted mean of the temperature at the PBX 9502 cylinder is shown in black.

Conclusions and Comments

The LHS runs of the SITI experiments 873, 875, 876, 877, and 878 determined that the most correlated parameter was the initial mass fraction of the adsorbed water, $U_{\omega h2oa}$. For the SITI experiments 874 and 880, the most correlated parameter was the enthalpy of reaction 2, $U_{h2.}$ Table 12 shows the values of the most correlated parameters for the all the SITI experiments considered in this study. Figure 49 plots the pressure measured by a static pressure transducer in the SITI experiments. Figure 49 shows that SITI tests 874 and 880 experienced leaks earlier than the rest of the experiments. Experiment 874 experienced the first leak at 2120 s and the SITI test 880 experienced a leak at 4280 s. According to the measurements shown in Figure 49, the pressure in SITI # 880 remained low from 4280 s up to the time of thermal ignition of 22417 s. This is probably why the most correlated parameter in SITI # 880 was the enthalpy of reaction 2, U_{h2}. The most correlated parameter in the SITI test 874 was the enthalpy of reaction 2, U_{h2}, but the initial mass fraction of the adsorbed water, $U_{\omega h2oa} = -0.438$, was also mildly correlated for this test. The SITI experiment 873 leaked and resealed about five times. These anomalies made the simulation of these experiments more challenging.

Table 12. Most correlated parameters obtained from the LHS simulations of the SITI experiments.

SITI #	Model Option	Correlation Coefficient
873	3	$U_{\omega h2oa} = -0.754$
875	4	$U_{\omega h2oa} = -0.600$
876	3	$U_{\omega h2oa} = -0.712$
877	4	$U_{\omega h2oa} = -0.617$
878	2	$U_{\omega h2oa} = -0.710$
874	4	$U_{h2} = -0.725$
880	Experimental Pressure[a]	$U_{h2} = -0.798$

[a] Pressure P in Eq. (10) was substituted by the experimental pressure shown in Fig. 5. This pressure data was used instead equation of state given by Eq. (12).

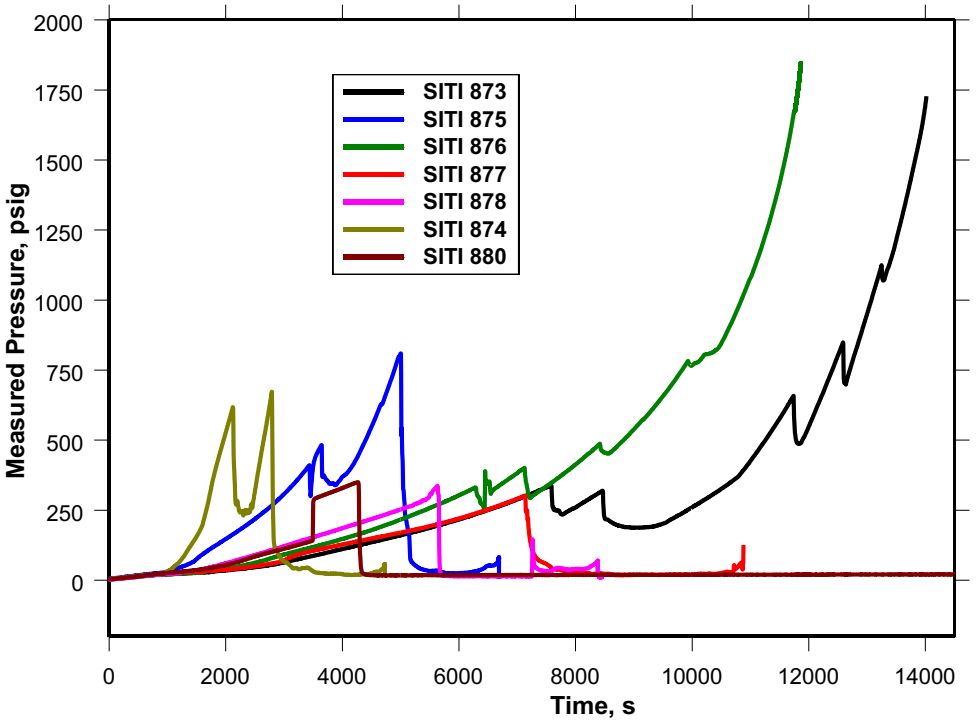

Figure 49. Measured static pressure in the SITI experiments.

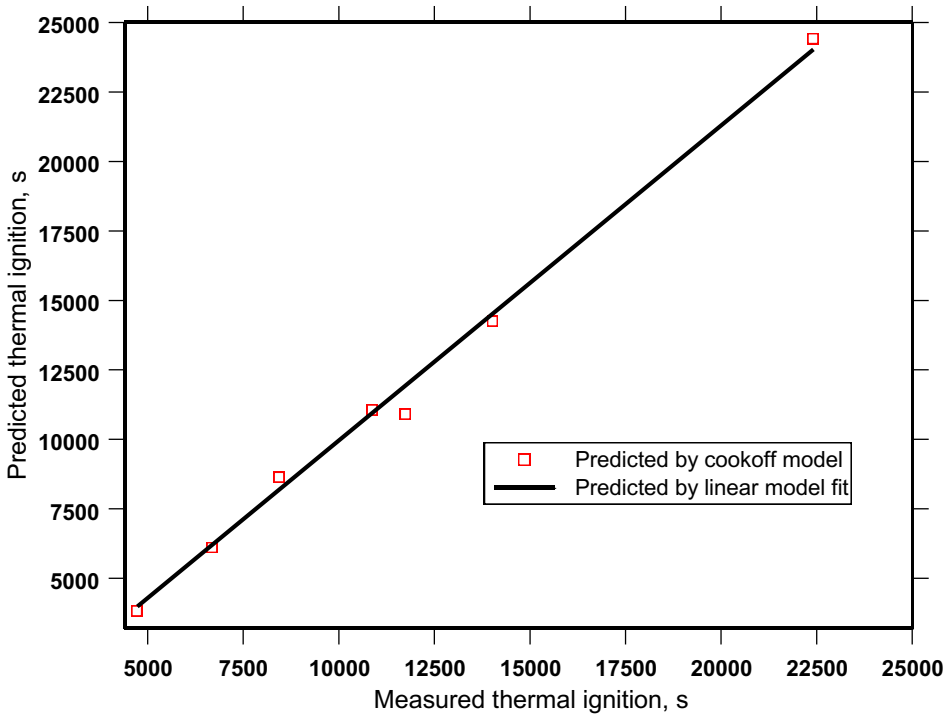

Figure 50. Measured against the LHS averages of the thermal ignition times for the 20 LHS simulations per experiment. The correlation coefficient is 0.993.

Table 13. Measured ignition times and LHS averages for the SITI experiments.

SITI #	873	874	875	876	877	878	880
Measured Ignition time, s	14034	4730	6696	11748	10881	8450	22417
LHS average, s	14281	3809	6804	10920	11040	8625	24383
Error, %	1.8	-19.5	-9.1	-7.0	1.5	2.1	8.8

The mean of the of the thermal ignition times produced by the 20 LHS simulations done for the each SITI experiment is given in Table 13. This table shows measured and calculated averages of the time-to-ignition as well as the percent error for all the SITI experiments considered. The range of errors is from -19.5% to +8.8% with an average error of -1.5%. The root mean squared deviation (RMSD) is 889 and the percent normalized RMSD is 5%. Figure 50 shows the measured ignition time plotted against the LHS averages of the thermal ignition time with a linear correlation coefficient of 0.993.

Acknowledgements

Daniel Trujillo, Q-15, had the initiative and provided the funding to carry out the SITI experiments considered in this report, and his contribution is gratefully acknowledged. The funding provided to write this report was provided by Daniel Trujillo, Q-15, and Nicholas Martinez, W-1, and this funding is also appreciated.

References

[1] Hobbs, M. L. and Kaneshige, M. J., J. *Chem. Phys.* 140, 124203 (2014).

[2] SIERRA Thermal/Fluid Development Team "SIERRA Multimechanics Module: Aria User Manual – Version 4.54," Sandia Report SAND2019-12296, Sandia National Laboratories, P. O. Box 5800, Albuquerque, New Mexico 87185, Livermore, California 94550, Printed October 9, 2019.

[3] Kaneshige, M. J.; Renlund, A. M.; Schmitt, R. G.; Erikson, W. W. Twelfth International Detonation Symposium; ONR 333-05-2; Office of Naval Research: San Diego, CA, 2002; p 821.

[4] Hobbs, M. L. and Baer, M. R., *Shock Waves* 2, 177 (1992).

[5] Maienschein, J. L. and Garcia, F., *Thermochim. Acta* 384, 71 (2002).

[6] Gibbs, T. R. and Popolato, A., *LASL Explosive Property Data* (University of California Press, Berkeley, CA, 1980), p. 124.

[7] Erikson, W. W., Cooper, M. A., Hobbs, M. L., Kaneshige, M. J., Oliver, M. S., Snedigar, S., "Determination of thermal diffusivity, conductivity, and energetic release from internal temperature profiles of energetic materials," *International Journal of Heat and Mass Transfer*, **79** (2014) 676–688.

[8] Wichman, I. S., "On the Use of Operator-Splitting Methods for the Equations of Combustion," *Combust. Flame*, 83, 240-252, 1991.

[9] McKay, M. D., Beckman, R. J., and Conover, W. J., Technometrics 21, 239 (1979).

[10] Adams, B. M., Bauman, L. E., Bohnhoff, W. J., Dalbey, K. R., Ebedia, M. S., Eddy, J. P., Eldred, M. S., Hough, P. D., Hu, K. T., Jakeman, J. D., Swiler, L. P., Vigil, D. M., DAKOTA, A Multilevel Parallel Object-Oriented Framework for Design Optimization, Parameter Estimation, Uncertainty Quantification, and Sensitivity Analysis: Version 5.4 User's Manual, SAND2010-2183, Sandia National Laboratories, Albuquerque, NM, 2010, updated 2013.